Lithospheric origin for Neogene-Quaternary Middle Atlas lavas (Morocco): Clues from trace elements and Sr-Nd-Pb-Hf isotopes

Delphine Bosch, René C. Maury, M. El Azzouzi, Claire Bollinger, Hervé Bellon, Patrick Verdoux

Lithospheric origin for Neogene–Quaternary Middle Atlas lavas (Morocco): Clues from trace elements and Sr–Nd–Pb–Hf isotopes

Delphine Bosch [a,*], René C. Maury [b], M'hammed El Azzouzi [b,c], Claire Bollinger [d], Hervé Bellon [b], Patrick Verdoux [e]

[a] UMR-UM2-CNRS 5243 Géosciences Montpellier, Université de Montpellier II, place E. Bataillon, c.c. 060, 34095 Montpellier, France
[b] UMR-CNRS 6538 Domaines océaniques, Institut Universitaire Européen de la Mer (IUEM), IUEM, Université de Brest, Université Européenne de Bretagne, place Nicolas Copernic, 29280 Plouzané, France
[c] Faculté des Sciences, Université Mohammed-V, av. Ibn Batouta, BP 1014, 10100 Rabat, Maroc
[d] UMS-CNRS 3113 Pôle de spectrométrie océan, IUEM, Université de Brest, Université Européenne de Bretagne, place Nicolas Copernic, 29280 Plouzané, France
[e] Laboratoire de Géochimie Isotopique environnementale, Université de Nîmes/Site GIS, UMR-CNRS 7330, rue Georges Besse, 30035 Nîmes Cedex 1, France

Keywords:
Intraplate alkali basalts
Middle Atlas mountains (Morocco)
Sr–Nd–Pb–Hf isotopes
Lithospheric mantle
HIMU geochemical flavour
Late Cretaceous metasomatism

abstract

This study presents new geochemical data on 26 mafic lavas from the Middle Atlas and Central Morocco volcanic provinces, including Miocene nephelinites and Pliocene–Quaternary (3.9–0.6 Ma) nephelinites, basanites, alkali and subalkaline basalts. Most of them represent near-primary magmas, although some alkali basalts were derived from the minor fractionation of olivine and diopside phenocrysts. These evolved samples and the subalkaline basalt display higher $^{207}Pb/^{204}Pb$ and Zr/Nb ratios and lower εNd consistent with their contamination by lower crustal granulites during an open fractionation process. The progressive enrichment in incompatible elements observed from alkali basalts to nephelinites suggests their derivation from decreasing partial melting degrees of an enriched mantle source located at the garnet–spinel transition zone. The strong negative spikes observed for K in multielement patterns indicate that this source contained a residual pargasitic amphibole. We propose that partial melting occurred at around 2 GPa, i.e. near the lithosphere–asthenosphere boundary beneath the Middle Atlas (60–80 km). The trace element and isotopic Sr–Nd–Pb–Hf signature of the uncontaminated lavas displays a geochemical flavour intermediate between those of high μ (HIMU), "C", and enriched mantle components. It is very similar to that of abundant metasomatic amphibole- and clinopyroxene-rich lithospheric peridotites and pyroxenites carried by Middle Atlas lavas, which likely represent an analog of the source of these lavas. It is therefore not necessary to postulate the contribution of a "fresh" asthenospheric mantle to their genesis. We propose that they resulted from the partial melting of the base of a veined lithospheric mantle metasomatised during the late Cretaceous by alkaline melts from the Central Atlantic plume, the ancestor of the Canary plume. Melting was probably triggered by the flux of a hot mantle within a regional SW–NE sub-lithospheric channel, in response to either the Alboran slab retreat or edge-driven convection around the West African craton.

1. Introduction

The origins and geodynamic controls of the Tertiary and Quaternary alkaline "anorogenic" mafic lavas from the circum-Mediterranean intracontinental volcanic provinces are still a matter of debate (see reviews by Wilson and Downes, 1992, 2006; Lustrino and Wilson, 2007; Lustrino et al., 2011). These provinces include alkali basalts and basanites, together with minor amounts of nephelinites and/or subalkaline basalts. These lavas display incompatible element enrichments and isotopic signatures similar to those of OIB basalts, usually with a high μ (HIMU) flavour. They occur in areas characterized by high geothermal gradients (fossil rifts and topographic bulges) and/or a thinned continental lithosphere underlain by an anomalously hot asthenospheric mantle (Bezada et al., 2013, 2014; Fullea et al., 2010). Their origin has often been attributed to the partial melting of the asthenospheric mantle forming either "genuine" deep-seated plumes (see Wilson and Downes, 1992, 2006, and Wilson and Bianchini, 1999, for a review) possibly emanating from a deep superplume (Forte et al., 2010); or uprising "splash plumes" (in the sense of Davies and Bunge, 2006) due to the accumulation of subducted oceanic slabs during the Mesozoic closure of the Tethys ocean (Carminati et al., 2012; Facenna and Becker, 2010; Lustrino and Wilson, 2007; Lustrino et al., 2011). Challenging models consider these mafic alkaline lavas as derived from the partial melting of a metasomatised subcontinental lithospheric mantle (e.g. Hawkesworth et al., 1990; Pilet et al., 2008, 2010). In the latter hypothesis the portion of the lithospheric mantle affected by melting processes would be chemically isolated from the convective (and eventually ascending) asthenospheric mantle, and thus should preserve the imprint of ancient depletion and/or refertilization events.

The origin of the Cantal (French Massif Central) alkali basalts and basanites illustrates this controversy. Indeed, the uprising asthenospheric plume imaged by Granet et al. (1995) and Sobolev et al. (1997) beneath this area is generally considered as their main source (Goes et al., 1999; Wilson and Downes, 2006). This asthenospheric flow was ascribed either to the detachment of the Alpine lithospheric root (Merle and Michon, 2001) or to the Apenninic slab roll-back (Barruol and Granet, 2002; Barruol et al., 2004). Alternatively, Pilet et al. (2004, 2008) considered that Cantal mafic alkaline lavas resulted from the melting of a metasomatised lithospheric subcontinental mantle containing amphibole- and clinopyroxene-rich veins, a hypothesis already proposed by Chauvel and Jahn (1984).

Such a debate is currently developing about the origin of the alkaline mafic lavas of the Middle Atlas Volcanic Province (MAVP) that is the largest and youngest volcanic field in Morocco (El Azzouzi et al., 2010; Frizon de Lamotte et al., 2008). They were considered as derived from the asthenospheric mantle (El Azzouzi et al., 1999) upwelling after a slab breakoff event (Coulon et al., 2002; Maury et al., 2000) or around the edges of a delaminating continental lithosphere (Bezada et al., 2014; Duggen et al., 2005). They overlie a SW–NE trending corridor of the thinned lithosphere (Missenard et al., 2006; Teixell et al., 2005) characterized by high thermal gradients (Fullea et al., 2010; Rimi, 2001). On the basis of their trace element and Sr–Nd–Pb isotopic similarities with Canary lavas, Duggen et al. (2009) proposed that they were derived from the melting of Canary mantle plume materials flowing NE along this corridor, more than 1500 km towards the western Mediterranean. This hypothesis does not account for several regional geological features (Berger et al., 2010) and an alternative model of asthenospheric convection around the edges of the neighbouring West African craton was proposed (Missenard and Cadoux, 2012). The petrologic and trace element study of 103 Middle Atlas lavas led El Azzouzi et al. (2010) to propose their derivation from amphibole-bearing metasomatised lithospheric mantle rocks, which occur as large xenoliths in some MAVP lavas (Malarkey et al., 2011; Natali et al., 2013; Raffone et al., 2009; Wittig et al., 2010a, 2010b).

The aim of this study is to investigate the asthenospheric vs. lithospheric origin of Middle Atlas lavas, based on the combination of trace element data and Sr, Nd, Pb and Hf isotopes on 26 representative mafic lavas from the MAVP and adjacent areas, together with previously published major element and petrographic data on the same samples (El Azzouzi et al., 2010). The results allow us to constrain some of the geodynamic processes controlling the Plio-Quaternary evolution of the western circum-Mediterranean regions.

2. Geological background and sampling

The Cenozoic volcanism of the Atlas Mountains is exclusively of intraplate alkaline type (Frizon de Lamotte et al., 2008) while in the Rif area it evolves through time from potassic calc-alkaline to shoshonitic and finally alkaline magmas (e.g. Coulon et al., 2002; Hernandez and Bellon, 1985; Maury et al., 2000). The Middle Atlas Volcanic Province (MAVP) belongs to an 800 km long SW–NE volcanic lineament stretching from the Siroua volcano in the Anti-Atlas Mountains towards the Mediterranean coast (inset in Fig. 1). This lineament crosscuts the major tectonic structures of central Morocco. It overlies a corridor of a thinned continental lithosphere, only 60–80 km thick beneath the MAVP (Missenard and Cadoux, 2012; Missenard et al., 2006), below which the asthenosphere is anomalously hot (Bezada et al., 2014; Fullea et al., 2010). The MAVP includes about one hundred well-preserved strombolian cones and maars (Fig. 1). These volcanoes have emitted numerous mafic lava flows covering a surface of ca. 960 km^2. However, the estimated volume of the MAVP is rather low (20 km^3) because of the limited thickness (usually 20–30 m) of the lava flow pile which overlies a rather flat Jurassic dolomitic limestone plateau (El Azzouzi et al., 2010). According to the surfaces they cover, dominant lava types (El Azzouzi et al., 1999, 2010) are alkali basalts (67.5%) and basanites (22.5%). Silica-saturated subalkaline basalts were defined according to the criterions set up by Middlemost (1975). They form the El Koudiate lapilli/scoria cone and associated flows which cover 7.8% of the MAVP (Fig. 1) and contain abundant quartz xenocrysts evidencing their contamination by African basement materials. These three lava types were erupted during the Plio-Quaternary (from 3.77 to 0.60 Ma, El Azzouzi et al., 2010). Nephelinites cover only 1.2% of the MAVP surface, and form small edifices emplaced during the Miocene (16.25–5.87 Ma) and the Plio-Quaternary, from 3.92 to 0.67 Ma (El Azzouzi et al., 2010; Harmand and Cantagrel, 1984). Alkali basalts, basanites and nephelinites are Mg-rich (8 wt.% b MgO b 13 wt.%) and display typical major and trace element characteristics of intra-plate ocean island basalts (OIB) and alkaline "anorogenic" intraplate continental igneous provinces (Lustrino and Wilson, 2007). These basalts show a strong negative K anomaly interpreted as indicating the presence in the source of residual K-rich hydroxyl-bearing minerals (amphibole or amphibole + phlogopite) (El Azzouzi et al., 2010). Considering the conditions of stability of pargasite (Niida and Green, 1999), this observation argues for the involvement of lithospheric mantle portions in the genesis of these lavas.

The present study deals with 9 nephelinites, 5 basanites, 8 alkali basalts and 1 subalkaline basalt (MA506) selected from the 103 MAVP samples described by El Azzouzi et al. (2010), who documented their precise locations (also shown in Fig. 1), petrographic features and ^{40}K–^{40}Ar ages. They were classified according to their position in the TAS diagram (Fig. 2). These samples were selected for their lack of post-magmatic minerals, low Loss On Ignition values, geological representativity (ages covering the whole range of activity of the MAVP) and geochemical diversity (Table 1). The four petrographic types contain 10–20 modal% olivine and calcic clinopyroxene phenocrysts, and their groundmass is either holocrystalline or microlitic. Nephelinites are feldspar-free, with nepheline occurring as microphenocrysts and amiboid patches in the groundmass. Interstitial nepheline and analcite are also present in the groundmass of basanites. Melilite has not been found in our samples, although this mineral has been identified in a few Middle Atlas and Central Morocco nephelinites (Harmand and Cantagrel, 1984; Rachdi et al., 1985). The 12 MAVP samples (2 nephelinites, 7 basanites and 3 alkali basalts) previously analyzed for Sr, Nd and Pb isotopes by Duggen et al. (2009) are shown for comparison in the geochemical plots presented below. In addition, we selected three samples (nephelinite KH36 and basanites KH33 and KH41) from a small volcanic field located ca. 80 km east of the MAVP, between the towns of Khenifra and Oulmes (Fig. 1), which is referred to as the Central Moroccan Volcanic Province (Frizon de Lamotte et al., 2008). It includes basanites and nephelinites whose ages and chemical features are similar to those of the MAVP (Rachdi et al., 1985). Sample KH36 was considered as a nephelinite despite its SiO_2 content of 41.40 wt.% (Fig. 3 and Table 1) because its feldspar-free mineral composition is similar to that of other nephelinites but for the occurrence of quartz xenocrysts. Basanite KH33 was dated at 0.98 ± 0.06 Ma by the ^{40}K–^{40}Ar method (El Azzouzi et al., 1999) and basanite KH41 and nephelinite KH36 at 1.00 ± 0.04 Ma and 1.67 ± 0.15 Ma, respectively (El Azzouzi, 2002).

3. Analytical methods

Rock samples were crushed then powdered in an agate mill for whole rock (WR) analyses. Major elements (Table 1) were analyzed by inductively coupled plasma-atomic emission spectrometry (ICP-AES) at IUEM, Plouzané using the methods described by Cotten et al. (1995). The international standards used for calibration were ACE, BEN, JB-2, PM-S and WS-E and the relative standard deviations are ±1% for SiO_2, and ±2% for other major elements except P_2O_5 and MnO (absolute precision ±0.01%). Samples were classified according to their position in the TAS diagram (El Azzouzi et al., 2010). During the present study, whole-rock trace element concentrations (Table 1)

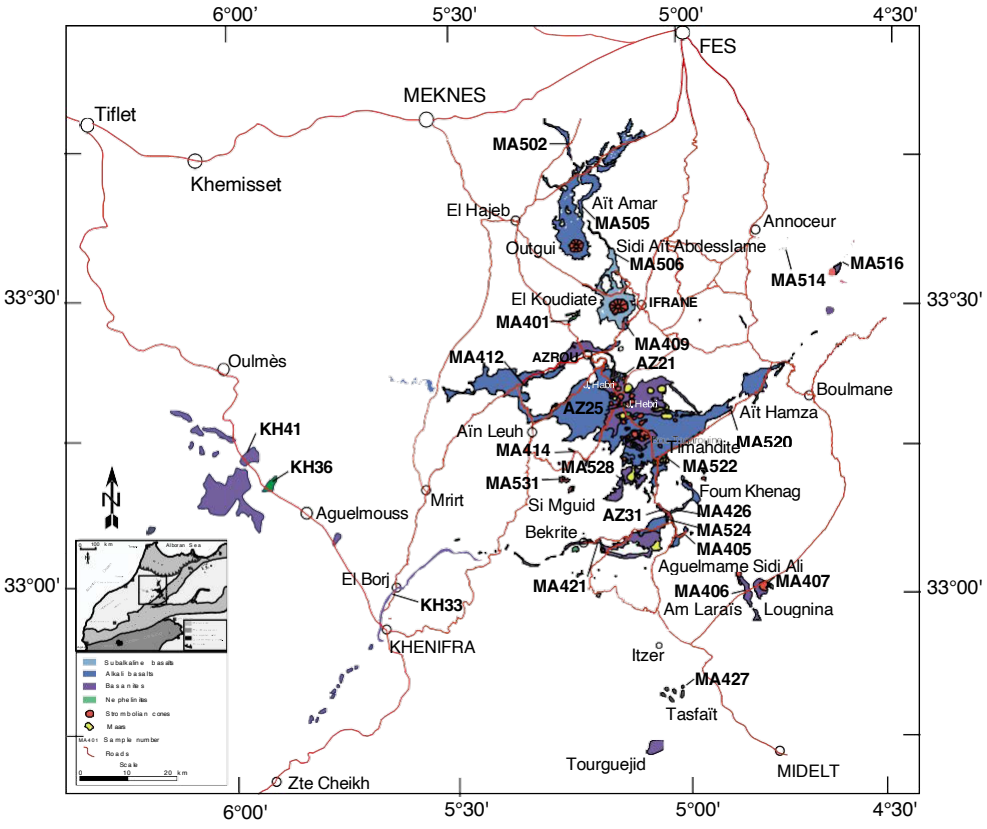

Fig. 1. Geological map of the Middle Atlas volcanic province and sampling sites showing the distribution of nephelinites, basanites, alkali basalts and subalkaline basalts (simplified from El Azzouzi et al., 2010). The locations of the studied samples are indicated with their specific numbers. Corresponding GPS positions are given in El Azzouzi et al. (2010). Inset: main tectonic structures of Morocco and locations of the Neogene and Quaternary volcanic districts.

were determined using a high resolution inductively coupled plasma mass spectrometer (ICP-MS) Thermo Element II at IUEM, Plouzané. Powders were completely dissolved, and elemental concentrations were calculated using the Tm addition method described in Barrat et al. (2007). Instrumental drift was corrected running a reference standard solution after every three samples. Based on standard measurements (see sample duplicates (Table 1) the 1σ analytical uncertainties are in most cases better than 4%. For the analyses of Sr–Nd–Pb–Hf isotopes, whole-rock powders were leached with 6 N HCl during 1 h at 95 °C and then rinsed three times with ultrapure water and centrifugated during 20 min for each step. After this leaching treatment, samples were dissolved during 72 h on a hot plate at 140 °C with a mixture of concentrated pure 48% HF and 13N HNO_3 acids (1:1) and small amounts of $HClO_4$. After evaporation to dryness, HNO_3 was added to the residue and kept at about 110 °C for 48 h before evaporation to dryness. The total blanks for Pb, Sr, Nd and Hf were respectively lower than 20 pg, 20 pg, 8 pg and 15 pg, respectively and were considered negligible for the present analyses. Pb was separated using anionic resin with HBr and HCl acids as reagents. Sr, Nd and Hf chemical separation was done using three successive concentration/purification steps for each element. The first one was the same for the three elements and was performed using cationic exchange resin. It consisted in a pre-concentration of, respectively, alkali, high field strength and rare earth elements. The two following steps were done, for each element, using specific Eichrom resins and following procedures modified after Pin et al. (1994) and Connelly et al. (2006). The Sr isotopic ratios were measured by thermal ionization mass spectrometry using a Triton Finnigan Mat spectrometer from the Labogis from the Nîmes University. Pb, Nd and Hf isotopic ratios were measured using the Nu-Instruments 500-HR MC–ICP-MS from the Ecole Normale Supérieure (ENS) of Lyon. To assess the reproducibility and accuracy of the isotopic ratios, standards were repeatedly run during this study. The standard average values were 0.710243 ± 10 (2σ) (n = 5) for the NBS987 Sr standard, 0.5119632 ± 4 (2σ) (n = 10) for the AMES-Rennes Nd standard and 0.282152 ± 13 (2σ) (n = 11) for the JMC-475 Hf standard. NBS981 Pb standards were routinely analyzed and yielded reproducibility better than 200 ppm for the three Pb dependant ratios. Isotopic ratios were either corrected for in situ radioactive decay using K–Ar ages obtained on the same samples (El Azzouzi et al., 2010), or uncorrected when no such ages were available (Table 2).

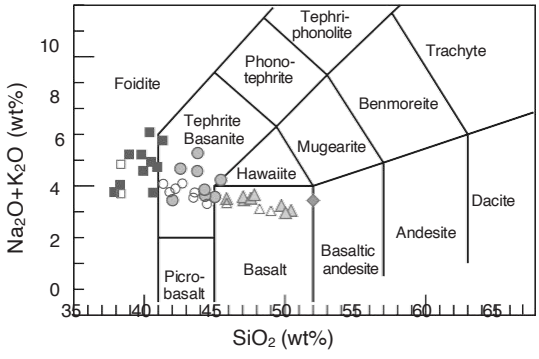

Fig. 2. Total alkalies versus silica plot (TAS) for Middle Atlas and Central Morocco alkaline lavas, according to Le Bas et al. (1986).

4. Results

4.1. Major and trace elements

Major elements were determined and discussed previously during the work of El Azzouzi et al. (2010), and only the most salient features

Table 1
Major and trace element compositions of Middle Atlas and Central Morocco alkaline lavas. Analytical methods detailed in the text.*: major elements and K–Ar age data from El Azzouzi et al. (2010).

Sample	MA401	MA414	MA427	MA514	MA522	MA524	MA531	KH36	AZ21
Location	Ariana flow	Ifri ou Berid	Tasfaït	Oued Soltane	Timahdite	Bekrite road	Si Mguid	Aguelmous	Michlifene
GPS coordinates	5°15′W–33°30′N	5°14′W–33°15′N	5°01′W–32°46′N	4°45′W–33°36′N	5°02′W–33°14′N	5°02′W–33°06′N	5°15′W–33°11′N		5°07′W–33°21′N
Age (Ma)*	15.62 ± 0.40	2.33 ± 0.10	16.25 ± 0.39	3.90 ± 0.11	0.67 ± 0.09	5.87 ± 0.16	14.72 ± 1.01	1.67 ± 0.15	0.75 ± 0.05
Rock-type	Nephelinite								
Major elements (wt.%)*									
SiO_2	40.60	40.50	38.30	39.00	39.85	40.90	37.95	41.40	40.00
Al_2O_3	11.60	11.82	12.15	11.28	11.16	12.15	12.20	13.95	11.90
Fe_2O_3*	13.40	13.55	12.00	12.55	12.88	12.85	11.70	14.50	13.40
MnO	0.20	0.23	0.21	0.23	0.20	0.21	0.21	0.22	0.21
MgO	12.30	10.00	10.05	11.35	11.78	11.40	11.18	6.61	11.45
CaO	12.50	11.60	15.10	14.50	13.00	12.40	16.00	11.35	12.60
Na_2O	3.30	5.20	3.52	4.26	4.40	4.06	3.46	4.43	3.85
K_2O	1.43	1.78	1.42	1.88	1.72	1.62	1.21	2.26	1.62
TiO_2	2.98	3.29	2.87	2.59	3.11	2.77	2.75	4.03	3.08
P_2O_5	1.12	1.15	1.85	1.19	1.11	1.14	1.53	1.42	1.25
LOI	0.00	0.37	1.48	0.95	0.02	0.00	1.27	0.00	0.22
Total	99.38	99.49	98.95	99.78	99.23	99.50	99.46	99.82	99.58
Trace elements (ppm)									
Li	10.30	11.20	–	12.40	7.60	9.30	9.20	11.90	–
Be	1.65	2.15	–	1.77	1.71	1.68	2.11	2.10	–
Rb	40.09	55.87	31.10	45.72	48.47	48.54	38.87	46.66	54.00
Sr	1195.20	1449.08	1820.00	1413.50	1315.09	1330.29	1452.47	1807.24	1380.00
Y	32.00	36.88	34.50	36.79	33.30	33.10	34.76	41.89	32.00
Zr	346.20	455.68	355.00	283.36	306.41	298.19	366.57	398.94	315.00
Nb	104.70	143.25	145.00	136.26	124.48	119.04	163.14	124.42	118.00
Cs	1.11	1.29	–	0.74	0.91	1.18	1.12	1.22	–
Ba	677.48	828.76	990.00	956.95	823.26	816.27	893.83	965.56	740.00
La	81.49	96.23	145.00	105.31	92.09	88.93	109.99	127.30	87.50
Ce	156.65	190.51	240.00	193.38	173.85	166.30	204.54	242.85	167.00
Pr	17.56	22.36	–	21.40	19.67	18.85	22.08	27.01	–
Nd	66.43	83.90	94.00	79.33	72.95	69.46	79.50	99.80	76.00
Sm	11.56	14.49	14.60	13.32	12.59	12.09	12.54	16.18	–
Eu	3.47	4.33	4.12	4.02	3.76	3.63	3.65	4.67	3.80
Gd	9.96	12.41	10.80	11.86	10.85	10.62	10.65	13.44	–
Tb	1.28	1.57	–	1.49	1.36	1.33	1.32	1.69	–
Dy	6.38	7.75	6.90	7.34	6.79	6.76	6.65	8.07	6.50
Ho	1.11	1.36	–	1.32	1.20	1.20	1.18	1.41	–
Er	2.69	3.30	3.00	3.19	2.96	2.99	3.01	3.45	2.90
Yb	2.03	2.48	2.48	2.38	2.21	2.26	2.40	2.55	1.93
Lu	0.28	0.34	–	0.32	0.30	0.31	0.33	0.34	–
Hf	7.18	9.51	–	5.76	6.40	6.07	6.64	8.13	–
Ta	6.62	9.06	–	7.04	7.40	6.93	9.49	7.61	–
W	1.40	2.80	–	1.65	2.38	2.10	2.74	3.56	–
Pb	3.98	4.58	–	2.87	2.64	3.85	2.46	6.50	–
Th	9.39	11.48	17.10	12.69	11.02	10.72	11.54	13.27	–
U	2.65	3.30	–	3.36	3.16	2.97	3.11	3.69	–
Sc	25.03	21.14	28.00	22.64	23.58	22.89	29.95	18.05	20.90
Ti	3.01	3.24	–	2.57	3.04	2.71	2.88	4.28	–
V	267.86	232.66	325.00	228.34	251.98	224.86	300.07	325.64	255.00
Cr	400.83	275.06	235.00	279.78	345.25	334.71	261.27	18.77	295.00
Mn	1486.69	1609.42	–	1669.72	1460.39	1499.83	1586.90	1709.03	–
Co	56.18	47.44	45.00	47.32	52.32	50.54	45.09	42.63	56.00
Ni	267.97	153.17	124.00	165.30	209.21	208.71	151.32	37.11	210.00
Cu	48.33	31.67	–	30.11	26.45	36.58	37.65	33.19	–
Ga	18.48	19.82	–	17.14	17.04	17.40	16.31	23.24	–
Zr/Nb	3.31	3.18	2.45	2.08	2.46	2.50	2.25	3.21	2.67
Zr/Hf	48.25	47.89	–	49.22	47.87	49.11	55.18	49.06	–
Nb/Ta	15.81	15.81	–	19.34	16.83	17.17	17.19	16.35	–
K/La	145.62	153.49	81.26	148.13	154.98	151.16	91.28	147.31	153.63
Ce/Pb	39.33	41.59	–	67.35	65.82	43.19	83.16	37.35	–
Hf/Sm	0.62	0.66	–	0.43	0.51	0.50	0.53	0.50	–
La_N/Yb_N	28.82	27.83	41.94	31.75	29.88	28.23	32.92	35.83	32.52
Ce_N/Yb_N	21.14	21.03	26.49	22.25	21.53	20.14	23.36	26.08	23.69
Dy_N/Yb_N	2.11	2.09	1.86	2.07	2.05	2.00	1.86	2.12	2.25

are outlined below. Most samples yield SiO_2 contents lower than 51 wt.% and are silica-undersaturated (normative nepheline), except subalkaline basalts, among which we selected only one sample, MA 506, which is characterized by a SiO_2 content of 52 wt.% (Table 1, Fig. 3). All samples display major element features typical of alkaline series with, in particular, a marked sodic tendency (Na_2O/K_2O N 3.8) and

AZ25	MA406	MA407	MA421	MA516	MA528	KH33	KH41	MA405	MA405dup
Jbel Tahabrit	Am Laraïs flow	Lougnina	Bekrite flow		Lechmine Bou Itguel	O. Oum Rabia	Oulmes	Aguelmane Sidi Ali	
5°08′W–33°18′N	4°52′W–33°00′N	4°51′W–33°00′N	5°12′W–33°04′N		5°07′W–33°11′N			4°59′W–33°04′N	
0.76 ± 0.07	1.56 ± 0.08	2.28 ± 0.013	1.65 ± 0.08		2.36 ± 0.029	0.98 ± 0.06	1.00 ± 0.04	2.27 ± 0.13	
	Basanite							Alkali basalt	
40.60	42.60	43.85	45.10	44.30	44.40	42.10	43.75	47.80	
11.80	12.65	13.24	13.20	11.70	12.90	12.30	12.80	13.60	
12.64	12.50	12.78	12.00	11.50	12.35	12.70	10.64	11.72	
0.19	0.19	0.19	0.17	0.17	0.18	0.19	0.18	0.17	
12.50	11.25	10.20	10.32	12.95	10.68	11.70	8.91	10.15	
11.30	11.00	10.40	10.60	9.00	10.70	11.60	11.90	9.18	
4.25	3.75	3.90	3.12	2.52	3.12	3.08	2.80	3.42	
1.60	1.91	1.60	1.40	2.24	1.42	1.28	3.42	1.14	
2.74	2.91	2.65	2.48	2.30	2.43	2.67	3.16	2.08	
1.02	0.94	1.04	0.68	0.80	0.78	0.83	0.67	0.52	
0.72	0.13	0.00	0.36	2.05	0.62	0.65	1.42	−0.49	
99.36	99.83	99.62	99.43	99.53	99.58	99.10	99.65	99.29	
8.00	10.20	9.70	12.60	–	11.70	7.90	8.40	14.90	14.70
1.64	1.70	1.68	1.31	–	1.40	1.35	1.77	1.21	1.18
37.17	48.15	39.71	33.91	49.60	36.45	31.11	90.86	29.34	28.97
1170.59	1160.28	1127.84	908.90	882.00	895.26	1304.09	1139.90	776.00	752.67
30.52	30.51	29.57	27.46	24.00	27.57	28.37	25.90	26.30	25.63
280.34	284.76	272.94	236.12	255.00	239.44	247.64	326.09	190.67	186.97
108.45	108.16	102.69	71.47	75.50	70.20	85.80	143.22	75.60	73.70
0.82	1.16	0.96	1.13	–	1.19	0.80	1.38	1.10	1.32
699.23	747.64	676.87	531.75	660.00	549.68	738.95	1005.54	384.83	378.04
79.18	75.95	78.94	49.57	62.00	54.18	61.81	76.81	41.93	41.25
147.98	142.27	144.75	99.62	110.00	105.52	119.56	158.03	84.21	81.37
16.16	15.84	15.60	11.74	–	12.29	13.77	18.34	9.77	9.69
60.72	59.54	57.67	45.65	46.00	47.11	52.98	68.18	37.99	37.69
10.64	10.69	10.02	8.81	9.00	8.86	9.74	10.41	7.58	7.42
3.24	3.21	3.03	2.72	2.60	2.73	2.99	2.94	2.36	2.34
9.31	9.24	8.93	8.08	7.10	8.14	8.80	8.28	6.99	6.87
1.21	1.22	1.16	1.07	–	1.07	1.15	1.04	0.98	0.95
6.11	6.14	5.89	5.53	4.90	5.61	5.80	5.13	5.14	5.03
1.08	1.08	1.05	0.99	–	1.00	1.03	0.93	0.94	0.92
2.67	2.65	2.58	2.44	2.10	2.50	2.48	2.35	2.34	2.32
2.01	1.98	1.94	1.83	1.68	1.91	1.86	1.97	1.82	1.81
0.27	0.27	0.27	0.25	–	0.26	0.25	0.27	0.25	0.25
5.67	5.97	5.31	5.03	–	5.23	5.27	7.08	4.25	4.13
6.42	6.60	5.80	4.49	–	4.28	5.15	9.17	4.79	4.67
2.17	2.02	1.62	1.19	–	1.44	1.36	1.47	0.81	0.81
3.28	3.98	4.05	3.49	–	3.61	2.96	4.80	3.66	3.56
9.23	9.61	9.35	5.77	–	6.58	6.96	9.08	4.84	4.73
3.05	3.10	2.56	1.58	8.95	1.74	1.76	2.49	2.52	2.47
22.36	23.74	20.15	21.55	17.00	21.56	22.27	27.28	20.41	20.18
2.72	2.93	2.62	2.44	–	2.39	2.61	3.01	2.04	2.03
221.45	237.76	212.48	201.91	182.00	203.70	222.32	294.55	167.98	166.68
402.74	336.42	255.68	339.54	544.00	317.48	339.86	336.92	294.32	289.96
1440.66	1390.84	1414.44	1244.96	–	1288.81	1348.87	1297.51	1244.98	1244.67
53.35	51.51	51.21	50.07	52.00	48.52	52.65	38.62	49.48	48.73
284.92	194.36	178.59	214.67	450.00	206.89	228.19	105.96	215.25	211.46
27.35	35.34	41.40	41.49	–	38.49	35.65	58.05	41.85	41.73
16.90	18.35	18.59	17.81	–	17.66	16.96	16.45	17.82	17.67
2.58	2.63	2.66	3.30	3.38	3.41	2.89	2.28	2.52	2.54
49.46	47.73	51.35	46.96	–	45.77	46.96	46.04	44.85	45.28
16.89	16.38	17.71	15.91	–	16.39	16.65	15.61	15.79	15.77
167.67	208.67	168.18	234.36	299.79	217.50	171.85	369.47	225.60	0.00
45.07	35.76	35.76	28.58	–	29.22	40.33	32.91	23.03	22.87
0.53	0.56	0.53	0.57	–	0.59	0.54	0.68	0.56	0.56
28.26	27.51	29.25	19.47	26.47	20.31	23.89	27.99	16.50	16.36
20.15	19.66	20.47	14.94	17.92	15.10	17.64	21.98	12.65	12.32
2.03	2.07	2.04	2.03	1.95	1.96	2.09	1.74	1.89	1.86

(*continued on next page*)

high TiO_2 contents (N 2.5 wt.%). Al_2O_3 increases from nephelinites towards alkali and subalkaline basalts (Fig. 3a), while CaO, TiO_2 and P_2O_5 decrease (Fig. 3b, c, d). The CaO/Al_2O_3 ratio remains high (N 0.6) for all samples but decreases slightly with increasing SiO_2 contents (Fig. 3e, f). Ni and MgO show a positive correlation (Fig. 4a), while Sc concentrations are not correlated with MgO contents (Fig. 4b). It is

Table 1 (*continued*)

Sample	MA409	MA412	MA426	MA502	MA502dup	MA505	MA520	AZ31	MA506
Location	Bou-Jirirh	Azrou–Mrirt	NNE Bou Angar	Bouderbala		Aït Amar	Aït Hamza	Foum Khenag	Sidi Aït Abdesslame
GPS coordinates	5°08′W–33°30′N	5°24′W–33°21′N	5°01′W–33°07′N	5°15′W–33°49′N		5°11′W–33°39′N	4°53′W–33°20′N	5°03′W–33°07′N	5°08′W–33°34′N
Age (Ma)*	3.77 ± 0.20	2.19 ± 0.18	2.74 ± 0.18	1.32 ± 0.39		0.89 ± 0.31	2.58 ± 0.12	0.60 ± 0.07	2.81 ± 0.22
Rock-type	Alkali basalt								Sub-alkali basalt
Major elements (wt.%)*									
SiO_2	45.80	50.00	47.50	47.00		50.50	49.70	47.10	52.00
Al_2O_3	12.25	14.05	13.60	13.70		13.86	13.90	13.98	14.43
Fe_2O_{3*}	12.00	11.30	11.70	12.05		11.20	11.55	11.63	10.60
MnO	0.20	0.16	0.17	0.17		0.16	0.17	0.19	0.15
MgO	12.00	8.92	9.90	9.30		7.79	8.75	9.80	6.76
CaO	10.00	8.92	9.58	9.82		9.25	9.50	9.75	8.75
Na_2O	3.12	3.03	3.25	3.25		3.11	3.20	3.15	3.15
K_2O	1.24	0.83	1.21	1.20		0.87	0.95	1.30	1.24
TiO_2	2.18	2.08	2.29	2.39		2.11	2.06	2.13	2.18
P_2O_5	0.89	0.44	0.58	0.55		0.45	0.50	0.70	0.42
LOI	0.05	−0.09	−0.02	−0.26		0.24	−0.41	−0.37	0.29
Total	99.73	99.64	99.76	99.17		99.54	99.87	99.36	99.97
Trace elements (ppm)									
Li	11.20	13.90	16.20	8.90	9.00	13.00	11.30	17.00	20.70
Be	1.44	1.06	1.45	1.18	1.16	1.24	0.93	1.47	1.55
Rb	32.67	20.59	29.81	29.47	29.59	22.52	19.33	37.79	38.32
Sr	1048.97	578.31	899.49	790.72	785.82	601.31	761.71	962.14	583.56
Y	30.09	24.21	27.89	26.47	26.41	25.36	26.14	29.11	25.84
Zr	248.42	181.05	227.40	217.18	215.67	182.63	183.26	224.85	196.09
Nb	81.38	40.62	89.98	69.00	68.91	39.01	75.73	89.51	41.30
Cs	1.13	1.03	0.92	0.56	0.58	1.06	0.07	1.59	2.13
Ba	617.65	288.62	452.66	419.09	417.50	329.81	309.00	518.86	330.17
La	77.87	29.57	50.22	39.02	38.85	32.80	35.50	57.95	31.06
Ce	141.77	61.36	100.60	79.44	79.06	64.08	75.35	111.80	64.51
Pr	15.58	7.47	11.65	9.65	9.76	7.70	9.24	12.53	7.82
Nd	57.35	30.14	44.94	38.12	38.64	31.01	36.84	47.51	31.65
Sm	9.93	6.48	8.46	7.82	7.76	6.51	7.42	8.75	6.73
Eu	3.00	2.08	2.59	2.46	2.49	2.11	2.40	2.69	2.12
Gd	8.77	6.34	7.75	7.37	7.27	6.51	6.99	7.94	6.58
Tb	1.16	0.90	1.05	0.98	1.00	0.90	0.97	1.08	0.91
Dy	6.02	4.82	5.47	5.12	5.22	4.86	5.12	5.67	4.83
Ho	1.09	0.88	0.97	0.92	0.95	0.90	0.94	1.03	0.89
Er	2.76	2.25	2.43	2.32	2.35	2.27	2.37	2.58	2.26
Yb	2.16	1.76	1.89	1.73	1.76	1.78	1.77	2.01	1.79
Lu	0.31	0.24	0.26	0.23	0.24	0.24	0.24	0.27	0.24
Hf	5.15	4.12	4.79	4.55	4.67	4.12	4.11	4.74	4.29
Ta	4.61	2.73	5.63	4.60	4.27	2.28	5.51	5.44	2.39
W	2.01	0.63	0.96	0.57	0.58	0.75	0.40	1.20	0.69
Pb	4.39	3.05	3.84	2.64	2.60	3.44	2.61	4.48	4.32
Th	9.66	3.75	5.70	4.23	4.25	4.20	3.62	6.92	4.38
U	2.67	1.34	2.58	1.91	1.97	1.24	0.98	2.69	1.86
Sc	20.30	20.54	21.39	21.68	21.65	21.07	21.43	22.07	20.58
Ti	2.07	2.05	2.36	2.42	2.39	2.13	2.08	2.15	2.18
V	183.54	166.04	186.64	198.37	199.10	163.29	174.33	185.52	172.81
Cr	443.73	328.72	305.69	297.02	303.28	301.74	309.38	327.03	232.33
Mn	1369.17	1116.99	1298.01	1268.89	1271.26	1137.04	1263.75	1321.04	1087.14
Co	50.03	45.79	49.34	48.95	49.81	43.55	46.38	47.29	38.86
Ni	313.96	182.05	210.36	188.76	189.63	165.34	177.58	195.54	116.65
Cu	38.97	27.33	35.03	36.85	37.12	34.56	21.41	32.66	31.77
Ga	16.37	17.74	18.43	18.71	18.97	18.69	18.64	18.58	19.66
Zr/Nb	3.05	4.46	2.53	3.15	3.13	4.68	2.42	2.51	4.75
Zr/Hf	48.20	43.95	47.46	47.77	46.23	44.29	44.55	47.43	45.69
Nb/Ta	17.65	14.91	15.99	15.00	16.13	17.12	13.75	16.44	17.27
K/La	132.13	232.88	199.94	255.21	0.00	220.09	222.05	186.16	331.28
Ce/Pb	32.30	20.11	26.18	30.04	30.40	18.62	28.88	24.98	14.93
Hf/Sm	0.52	0.64	0.57	0.58	0.60	0.63	0.55	0.54	0.64
La_N/Yb_N	25.83	12.08	19.08	16.22	15.85	13.25	14.35	20.71	12.47
Ce_N/Yb_N	17.95	9.56	14.58	12.60	12.31	9.88	11.63	15.25	9.89
Dy_N/Yb_N	1.86	1.84	1.94	1.99	1.99	1.83	1.93	1.89	1.81

noteworthy that the nephelinites encompass all the range of variation of the Ni and Sc contents (Fig. 4) measured on the twenty-six studied lavas (Table 1) and the twelve samples from Duggen et al. (2009).

The Middle Atlas lavas show light rare earth element (LREE)-enriched chondrite-normalized patterns with a roughly fan-shaped tendency similar to those of many ocean island basalts (OIB) and alkaline

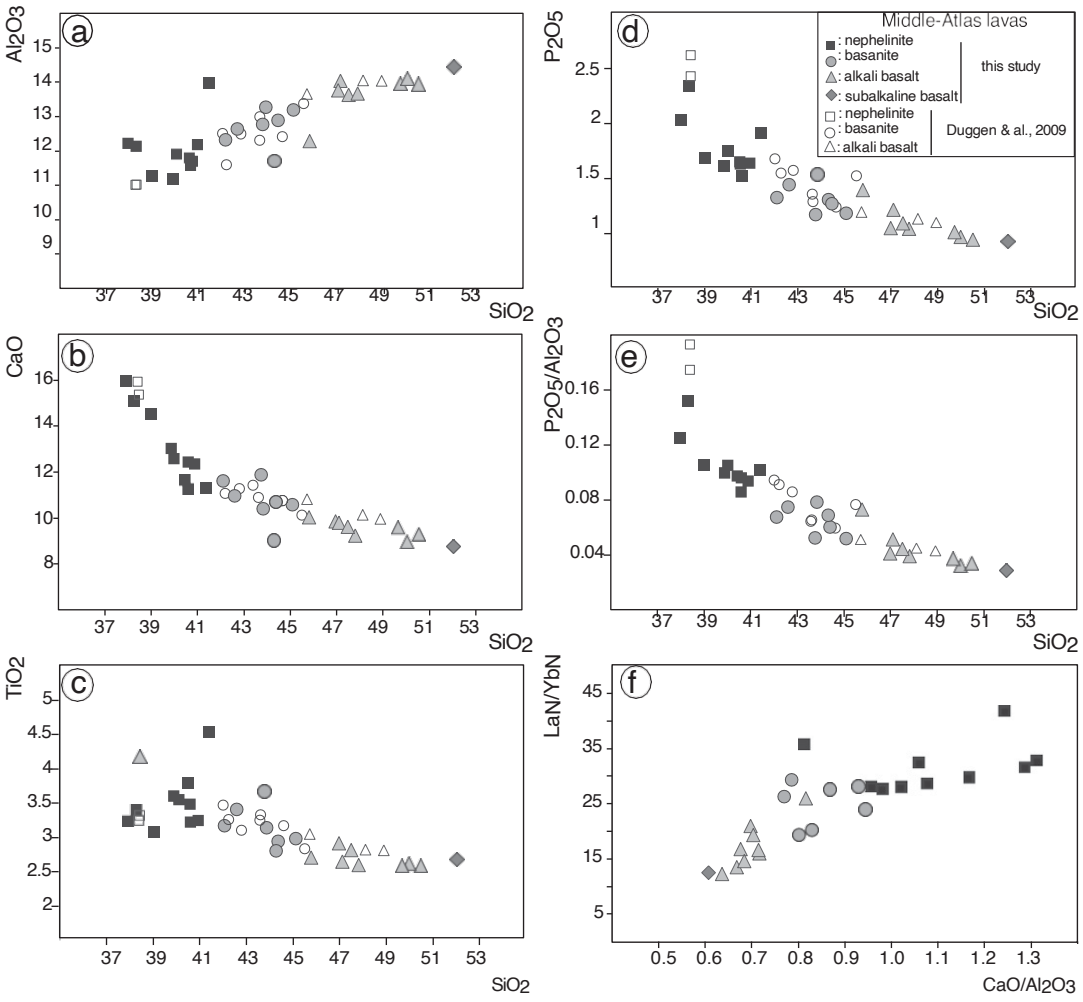

Fig. 3. Major element (wt.%) diagrams for the studied Middle Atlas and Central Morocco lavas. a: Al_2O_3 versus SiO_2; b: CaO versus SiO_2; c: TiO_2 versus SiO_2; d: P_2O_5 versus SiO_2; e: P_2O_5/Al_2O_3 versus SiO_2; f: La_N/Yb_N versus CaO/Al_2O_3. Duggen et al.'s (2009) data on 12 MAVP samples analyzed for major, trace elements and Sr, Nd, Pb isotopes are reported for comparison (open symbols). La/Yb ratios are normalized using chondritic values from Sun and McDonough (1989).

volcanic rocks from continental settings (Fig. 5a, Table 1). No marked Eu anomaly is noticeable and, combined with the increasing Al_2O_3 content from nephelinites to alkali basalts (Fig. 3a), this feature suggests that plagioclase was not a major fractionating mineral phase at this stage. Another interesting feature is the strong overlap in both compatible and incompatible element concentrations measured in nephelinites, basanites, alkali and subalkaline basalts (Table 1 and Figs. 4 and 5). In the primitive mantle-normalized multi-element diagrams all the studied samples show similar patterns with significant enrichments in incompatible elements and strong negative K and Pb spikes (Fig. 5b). However, (La_N/Yb_N) ratios tend to decrease progressively (Fig. 3f) from nephelinites (28–42) towards basanites (19–28) and alkali basalts (12–26). Subalkaline basalt MA506 shows the lowest (La_N/Yb_N) ratio (12) measured during the present study. Such mafic magma patterns are typical of continental intraplate volcanism, and are commonly documented, for example, in central Europe and in the circum-Mediterranean areas (see Lustrino and Wilson, 2007 and Lustrino et al., 2011 for a review). The sample patterns show maxima for Nb and Ta together with high values for their neighbours U, Th and La, whereas strong negative anomalies are observed for Pb and K relative to elements of similar incompatibility (Fig. 5b). A small trough is also present at the level of Zr and Hf.

4.2. Isotopes

The initial $^{87}Sr/^{86}Sr$ and $^{143}Nd/^{144}Nd$ ratios of the 26 analyzed samples show significant ranges of variation extending from 0.70315 to 0.70411 and from 0.51275 to 0.51292, respectively (Table 2). The first range is reduced to 0.70315–0.70382 excluding subalkaline basalt MA506, which is characterized by the highest $^{87}Sr/^{86}Sr$ ratio. The corresponding εSr and εNd values, from −19.10 to −9.62 and from + 2.23 to + 5.49 respectively, are typical of an enriched mantle source [http://georoca.mpch-mainz.gwdg.de/georoc/]. In the Nd–Sr isotopic diagram (Fig. 6a), the samples define a relatively large domain located in the depleted area relative to Bulk Earth (CHUR) and partly overlapping both worldwide MORB and OIB fields. Although the different types of lavas partly overlap, subtle variations from more depleted to slightly more enriched ratios can be detected between nephelinites, basanites and alkali basalts. Overall, the analyses define an elongated trend stretching from depleted compositions similar to the European Asthenospheric Reservoir (EAR, Cebria and Wilson, 1995) towards Bulk Earth (CHUR) values (Fig. 6a). Within this trend, the alkali and subalkaline basalts tend to display slightly more radiogenic $^{87}Sr/^{86}Sr$ and $^{143}Nd/^{144}Nd$ values compared to other lithologies. This trend is roughly similar to those defined for Cenozoic alkaline intra-plate lavas

Table 2

Sr, Nd, Pb and Hf isotopic compositions of Middle Atlas and Central Morocco alkaline lavas. Analytical methods are detailed in the text. The Sr, Nd and Hf isotope ratios were normalized to $^{86}Sr/^{88}Sr = 0.1194$, $^{146}Nd/^{144}Nd = 0.7219$ and $^{179}Hf/^{177}Hf = 0.7325$, respectively. The 2 SE values refer to within-run precisions, given as standard errors on the mean (SE) quoted at the 95% confidence level. Rb, Sr, Sm, Nd, Lu, Hf, U, Th and Pb concentrations (ppm) were measured with precision estimated to 1%. εSr, εNd, εHf values were calculated as the deviation from a chondritic uniform reservoir (CHUR) with present-day $^{86}Sr/^{87}Sr = 0.70448$–$^{87}Rb/^{85}Rb = 0.0816$, $^{143}Nd/^{144}Nd = 0.512638$–$^{147}Sm/^{144}Nd = 0.1966$, $^{176}Hf/^{177}Hf = 0.282772$–$^{176}Lu/^{177}Hf = 0.0332$ (Blichert-Toft and Albarède, 1997; Jacobsen and Wasserburg, 1980).

Sample	MA401	MA414	MA427	MA514	MA522	MA524	MA531	KH36	AZ21	AZ25
Location	Ariana flow	Ifri ou Berid	Tasfaït	Oued Soltane	Timahdite	Bekrite road	Si Mguid	Aguelmous	Michlifene	Jbel Tahabrit
GPS coordinates	5°15′W–33°30′N	5°14′W–33°15′N	5°01′W–32°46′N	4°45′W–33°36′N	5°02′W–33°14′N	5°02′W–33°06′N	5°15′W–33°11′N		5°07′W–33°21′N	5°08′W–33°18′N
Age (Ma)	15.62 ± 0.40	2.33 ± 0.10	16.25 ± 0.39	3.90 ± 0.11	0.67 ± 0.09	5.87 ± 0.16	14.72 ± 1.01	1.67 ± 0.15	0.75 ± 0.05	0.76 ± 0.07
Rock-type	Nephelinite									
$^{87}Rb/^{86}Sr$	0.097	0.111	0.049	0.094	0.107	0.106	0.077	0.075	0.113	0.114
$^{87}Sr/^{86}Sr$	0.703223 ± 8	0.703205± 8	0.703216 ± 5	0.703164 ± 5	0.703210 ± 11	0.703153 ± 5	0.703237 ± 8	0.703455 ± 8	0.703194± 4	0.703155 ± 5
$^{87}Sr/^{86}Sr_{(i)}$	0.703202	0.703199	0.703216	0.703159	0.70321	0.703146	0.703221	0.70345	0.70319	0.70315
εSr	−18.13	−18.39	−18.23	−18.96	−18.31	−19.12	−17.93	−14.83	−18.54	−19.10
$εSr_{(i)}$	−18.17	−18.40	−17.96	−18.97	−18.31	−19.14	−17.92	−14.83	−18.53	−19.10
$^{147}Sm/^{144}Nd$	0.105	0.104	0.094	0.101	0.104	0.105	0.095	0.098	–	0.111
$^{143}Nd/^{144}Nd$	0.512841 ± 6	0.512894 ± 3	0.512844 ± 5	0.512873 ± 2	0.512880 ± 6	0.512922 ± 7	0.512856 ± 5	0.512788 ± 4	0.512856 ± 2	0.512866 ± 3
$^{143}Nd/^{144}Nd_{(i)}$	0.51283	0.51289	0.512844	0.51287	0.51288	0.51292	0.51285	0.51279	–	0.51286
εNd	3.96	4.99	4.02	4.58	4.72	5.54	4.25	2.93	4.25	4.45
$εNd_{(i)}$	3.79	4.96	4.06	4.54	4.71	5.49	4.11	2.91	–	4.44
$^{176}Lu/^{177}Hf$	0.005	0.005	–	0.007	0.007	0.007	0.007	0.006	–	0.008
$^{176}Hf/^{177}Hf$	0.282988 ± 3	0.282972 ± 3	0.282942 ± 3	–	0.282976 ± 5	0.282973 ± 2	0.282913 ± 3	0.282935 ± 3	–	0.282978 ± 3
$^{176}Hf/^{177}Hf_{(i)}$	0.28299	0.28297	–	–	0.28297	0.28297	0.28291	0.28293	–	0.28298
εHf	7.65	7.07	6.02	–	7.20	7.11	4.97	5.76	–	7.28
$εHf_{(i)}$	7.59	7.06	–	–	7.20	7.09	4.90	5.75	–	7.27
$^{206}Pb/^{204}Pb$	19.6324 ± 3	19.8207 ± 3	19.9713 ± 3	19.4182 ± 6	19.5738 ± 4	19.6820 ± 4	20.2773 ± 5	19.6986 ± 6	19.8408 ± 4	19.5807 ± 5
$^{207}Pb/^{204}Pb$	15.6270 ± 2	15.6201 ± 3	15.6246 ± 3	15.6375 ± 5	15.6248 ± 3	15.6249 ± 3	15.6456 ± 4	15.6291 ± 5	15.6225 ± 3	15.6201 ± 7
$^{208}Pb/^{204}Pb$	39.3604 ± 7	39.4222 ± 8	39.7659 ± 8	39.2638 ± 13	39.2823 ± 7	39.3952 ± 14	39.8937 ± 15	39.5286 ± 16	39.4876 ± 10	39.2960 ± 19
$^{206}Pb/^{204}Pb_{(i)}$	19.529	19.800	19.971	19.373	19.566	19.644	20.088	19.688	19.841	19.576
$^{207}Pb/^{204}Pb_{(i)}$	15.622	15.619	15.625	15.635	15.624	15.623	15.637	15.629	15.623	15.620
$^{208}Pb/^{204}Pb_{(i)}$	39.238	39.397	39.766	39.207	39.273	39.350	39.661	39.516	39.488	39.292

from other circum-Mediterranean provinces, e.g. the French Massif Central, Languedoc, Catalogna (Dautria et al., 2010; Lustrino and Wilson, 2007; Wilson and Downes, 2006). The Hf isotopes define a range of variation from 0.28282 to 0.28302 (+1.66 ≤ εHf ≤ +8.90; Table 2). This range can be significantly reduced to +4.90 ≤ εHf ≤ +8.90 if we exclude basanite KH41 from Central Morocco. When plotted in the Nd–Hf isotope diagram (Fig. 6b), the samples straddle the oceanic mantle array, partly overlapping the worldwide MORB and OIB fields or lying below it at lower εHf. Together, they define a domain located between the HIMU and DMM components (Zindler and Hart, 1986) without a really discernable difference between the different types of lavas (Fig. 6b). Basanite KH41 yields significantly lower εHf and εNd values, which will be discussed below. All samples show significantly enriched Pb isotopic ratios ranging from 19.101 to 20.270, from 15.604 to 15 .676 and from 38.969 to 40.052 for $^{206}Pb/^{204}Pb$, $^{207}Pb/^{204}Pb$ and $^{208}Pb/^{204}Pb$, respectively (Table 2). These ratios are highly scattered and a majority of samples (including all the nephelinites and basanites) define a linear array sub-parallel to the Northern Hemisphere Reference Line (NHRL) in Fig. 7a. It is noteworthy that alkali and subalkaline basalts are characterized by significantly higher $^{207}Pb/^{204}Pb$ and lower $^{206}Pb/^{204}Pb$ ratios than the other samples, and tend to plot away from the NHRL (Fig. 7a, b).

5. Discussion

5.1. Role of fractional crystallization

Most of the studied nephelinites, basanites and alkali basalts have MgO (≥ 8–9 wt.%) and Ni contents (≥ 150 ppm) high enough (Fig. 4) to consider that they represent near-primary magmas (e.g. Allègre et al., 1977; Frey et al., 1978). This feature is also consistent with the occurrence of mantle xenoliths in a number of these flows and the lack of intermediate and evolved lavas in the MAVP (El Azzouzi et al., 2010).

Nevertheless, decreasing CaO and TiO_2 contents with increasing Al_2O_3 and SiO_2 is consistent with a minor accumulation/fractionation of diopside (Fig. 3b, c). This mineral is the most abundant phenocryst in MAVP nephelinites and the second one (after olivine) in basanites and alkali basalts. The positive correlation between Ni and MgO contents is also consistent with olivine fractionation/accumulation (Fig. 4a). However, Sc contents plotted against MgO do not show the decreasing trend commonly attributed to clinopyroxene fractionation/accumulation, which is thus considered as minor (Fig. 4b). One nephelinite from Central Morocco (KH36) differs from the other samples by its significantly lower MgO, Ni and Cr contents (Fig. 4 and Table 1). This feature suggests that its parental magma experienced more olivine + clinopyroxene fractionation than the others. However, a number of geochemical features of the Middle Atlas lavas cannot be explained by fractional crystallization of olivine and/or clinopyroxene. For instance, nephelinites and basanites have rather similar MgO contents (Fig. 4) but the former displays consistently higher incompatible element concentrations (Fig. 5). Similarly, the wide range of CaO contents (Fig. 3b) measured for nephelinites, that are characterized by high MgO contents (≥ 10 wt.%, except KH36), is consistent with source compositional variations. Thus, a closed-system fractional crystallization process cannot account for the geochemical variations observed between the different lava types. An open-system fractionation process coupled with high degrees of crustal contamination from the local basement (see Section 5.3 below), would additionally result in an increase of Rb, Ba, and Th contents and in high $^{87}Sr/^{86}Sr$ ratios coupled with low $^{143}Nd/^{144}Nd$ and $^{176}Hf/^{177}Hf$ ratios, which are not observed in a large majority of the studied samples (Tables 1 and 2).

5.2. Partial melting and source mineralogy

The composition of primary mantle melts depends on the chemical composition and mineralogy of the mantle, and on the degree and

MA406	MA407	MA421	MA516	MA528	KH33	KH33 dup.	KH41	KH41 dup.
Am Laraïs flow	Lougnina	Bekrite flow		Lechmine Bou Itguel	O. Oum Rabia	O. Oum Rabia	Oulmes	Oulmes
4°52′W–33°00′N	4°51′W–33°00′N	5°12′W–33°04′N		5°07′W–33°11′N				
1.56 ± 0.08	2.28 ± 0.013	1.65 ± 0.08		2.36 ± 0.029	0.98 ± 0.06	0.98 ± 0.07	1.00 ± 0.04	1.00 ± 0.05
Basanite								
0.120	0.102	0.108	0.029	0.118	0.069	0.069	0.230	0.230
0.703235 ± 9	0.703199 ± 6	0.703479 ± 4	0.703338 ± 4	0.703442 ± 7	0.703211 ± 6	0.703227 ± 5	0.703654 ± 10	0.703672 ± 10
0.70323	0.70319	0.70347	0.70334	0.70344	0.70321	0.70323	0.70365	0.70367
−17.96	−18.47	−14.49	−16.48	−15.02	−18.30	−18.07	−12.00	−11.75
−17.97	−18.48	−14.50	−16.47	−15.03	−18.29	−18.05	−12.04	−11.80
0.108	0.105	0.116	0.118	0.114	0.111	0.111	0.092	0.092
0.512852 ± 5	0.512857 ± 4	0.512852 ± 4	0.512840 ± 3	0.512818 ± 5	0.512837 ± 6	0.512843 ± 5	0.512753 ± 6	0.512724 ± 8
0.51285	0.51286	0.51285	0.51284	0.51282	0.51284	0.51284	0.51275	0.51272
4.17	4.27	4.17	3.94	3.51	3.88	4.00	2.24	1.68
4.16	4.25	4.15	3.94	3.48	3.87	3.99	2.23	1.67
0.006	0.007	–	–	0.007	0.007	–	0.005	–
0.283024 ± 11	0.282982 ± 2	–	–	0.282944 ± 3	0.282983 ± 2	–	0.282819 ± 8	–
0.28302	0.28298	–	–	0.28294	0.28298	–	0.28282	–
8.91	7.43	–	–	6.09	7.46	–	1.66	–
8.90	7.42	–	–	6.07	7.46	–	1.66	–
19.5229 ± 2	19.5565 ± 3	19.2592 ± 4	19.9122 ± 10	19.2833 ± 4	19.4829 ± 8	19.4684 ± 29	20.2745 ± 3	20.2696 ± 3
15.6226 ± 3	15.6052 ± 3	15.6366 ± 3	15.6340 ± 8	15.6365 ± 4	15.6199 ± 7	15.6065 ± 25	15.6762 ± 3	15.6737 ± 2
39.3193 ± 7	39.3097 ± 12	39.2689 ± 9	39.5924 ± 15	39.2398 ± 11	39.2938 ± 10	39.2765 ± 66	40.0584 ± 9	40.0505 ± 6
19.511	19.542	19.2518	19.912	19.272	19.477	19.463	20.269	20.270
15.622	15.604	15.636	15.634	15.636	15.620	15.606	15.676	15.674
39.307	39.292	39.260	39.592	39.226	39.286	39.269	40.052	40.050

(*continued on next page*)

mode of partial melting. The progressive enrichment in incompatible elements observed from alkali basalts to nephelinites suggests a decreasing partial melting degree of an enriched mantle source (Langmuir et al., 1992). Ratios of incompatible elements, for instance P_2O_5 versus Al_2O_3, can be used to decipher between different degrees and varying depths of melting. Indeed, Al_2O_3 content is largely controlled by spinel or garnet during mantle melting and thus the P_2O_5/Al_2O_3 ratio increases with an increasing depth of melting (Furman, 1995). Alkali and subalkaline basalts show higher SiO_2 and distinctly lower P_2O_5/Al_2O_3 ratios than basanites and nephelinites. The higher P_2O_5/Al_2O_3 and La_N/Yb_N ratios of nephelinites with respect to other rock types are consistent with lower melting degrees of garnet- or spinel-bearing sources (Fig. 3e, f). The strong fractionation of HREE (Dy_N/Yb_N N 1.7; Table 1) further indicates that the primitive MAVP lavas represent the partial melts of a mostly garnet-bearing source. Therefore, major and trace element data suggest that the nephelinite–basanite–alkali basalt sequence originated from rather similar LREE-enriched sources (Fig. 5), and that nephelinitic magmas correspond to lower-degree partial melts probably formed at deeper average melting depths given their higher La_N/Yb_N ratios (Fig. 3f). Alkali basalts would represent higher degrees of partial melting at shallower average depths. The concomitant emplacement of nephelinitic, basanitic and alkali basaltic lavas from ca. 5.9 to 0.6 Ma (El Azzouzi et al., 2010) suggests that large variations of melting conditions occurred simultaneously in the MAVP mantle.

We tentatively used the REE composition parameters (e.g. Dy_N/Yb_N versus Ce_N/Yb_N) to model the partial melting degree of a regional mantle source from the garnet stability field and garnet–spinel transition zone (Haase et al., 2004) (Fig. 8a). The modelling shows that samples could be derived from about 2% (nephelinite) to 7–8% (alkali basalts) partial melting degrees, mainly in the garnet–spinel peridotite transition zone. These results are consistent with those deduced from La/Yb versus Yb plots using Luhr et al.'s (1995) plots (El Azzouzi et al., 2010). Three samples, one basanite (KH41) and two nephelinites (MA427 and MA531), plot below the intermediate spinel–garnet stability field in Fig. 8a, suggesting a spinel–peridotite source for these lavas. The REE melting model suggests that the mantle source of the Middle Atlas lavas must have been enriched in LREE (e.g. Ce) to fit partial melting degrees of ca. 2–7%. Moreover, positive correlations between the Ce_N/Yb_N ratio and Ce and Yb contents indicate that this source was probably intermediate between spinel and garnet-bearing peridotite (Fig. 8b, c). The transition from garnet to spinel occurs between 1.8 and 2.2 GPa for typical lherzolite compositions at ca. 1300 °C according to experimental data (Klemme and O'Neill, 2000; Walter et al., 2002) and studies carried on Hawaiian mantle xenoliths (Sen et al., 2005). It is thus reasonable to assume that partial melting at the origin of the MAVP lavas occurred under pressures close to 2 GPa, corresponding to a depth around 65 km given the Middle Atlas crustal thickness (31 km according to Ayarza et al., 2014) and densities determined by Fullea et al. (2010). This depth fits that of the lithosphere–asthenosphere boundary which is located at 60–80 km beneath the Middle Atlas (Fullea et al., 2010; Miller and Becker, 2014; Missenard et al., 2006; Teixell et al., 2005).

In addition, the nephelinite–basanite–alkali basalt MAVP suite defines a negative correlation in the K/La versus Ce_N/Yb_N plot (Fig. 8d). This feature implies that low degrees of partial melting of garnet and/or spinel peridotite cannot fully account for the measured K/La and Ce/Yb ratios (Haase et al., 2004). A residual mineral phase fractionating K with respect to La was therefore necessarily present. The strong negative spikes observed for K in multi-element diagrams (Fig. 5b), combined with the relative depletion of medium rare earth elements (MREE) relative to the light (LREE) and heavy rare earth elements (HREE) (Fig. 5a), are consistent with the presence of residual amphibole in the source region of the MAVP magmas (Class and Goldstein, 1997; Panter et al., 2006). The presence in their source of residual pargasitic amphibole which experiences dehydration melting under pressures slightly lower than 2 GPa (Niida and Green, 1999; Spath et al., 2001)

Table 2 (*continued*)

Sample	MA405	MA405dup	MA409	MA412	MA426	MA502	MA505	MA520	AZ31	MA506
Location	Aguelmane Sidi Ali	Aguelmane Sidi Ali	Bou-Jirirh	Azrou–Mrirt	NNE Bou Angar	Bouderbala	Aït Amar	Aït Hamza	Foum Khenag	Sidi Aït Abdesslame
GPS coordinates	4°59′W–33°04′N	4°59′W–33°04′N	5°08′W–33°30′N	5°24′W–33°21′N	5°01′W–33°07′N	5°15′W–33°49′N	5°11′W–33°39′N	4°53′W–33°20′N	5°03′W–33°07′N	5°08'W–33°34'N
Age (Ma)	2.27 ± 0.13	2.27 ± 0.13	3.77 ± 0.20	2.19 ± 0.18	2.74 ± 0.18	1.32 ± 0.39	0.89 ± 0.31	2.58 ± 0.12	0.60 ± 0.07	2.81 ± 0.22
Rock-type	Alkali basalt									Sub-alkali basalt
$^{87}Rb/^{86}Sr$	0.109	–	0.090	0.103	0.096	0.108	0.108	0.073	0.069	0.190
$^{87}Sr/^{86}Sr$	0.703566 ± 10	–	0.703371 ± 5	0.7038197 ± 8	0.703598 ± 5	0.703235 ± 5	0.703696 ± 12	0.703616 ± 6	0.703643 ± 5	0.704122 ± 12
$^{87}Sr/^{86}Sr_{(i)}$	0.70356	–	0.70337	0.70382	0.70359	0.70323	0.70369	0.70361	0.70364	0.70411
εSr	−13.26	–	−16.06	−9.66	−12.84	−17.95	−11.41	−12.55	−12.17	−5.36
$εSr_{(i)}$	−13.27	–	−16.03	−9.62	−12.81	−17.97	−11.41	−12.54	−12.17	−5.43
$^{147}Sm/^{144}Nd$	0.120	0.119	0.104	0.130	0.114	0.124	0.127	0.122	0.111	0.128
$^{143}Nd/^{144}Nd$	0.512803 ± 3	0.512796 ± 6	0.512863 ± 4	0.512813 ± 7	0.512896 ± 12	0.51289 ± 5	0.512805 ± 5	0.512809 ± 6	0.512808 ± 8	0.512764 ± 8
$^{143}Nd/^{144}Nd_{(i)}$	0.51280	0.51279	0.51286	0.51281	0.51289	0.51289	0.51280	0.51281	0.51281	0.51276
εNd	3.22	3.08	4.39	3.41	5.03	4.97	3.26	3.34	3.32	2.46
$εNd_{(i)}$	3.19	3.05	4.35	3.38	4.99	4.96	3.25	3.30	3.31	2.42
$^{176}Lu/^{177}Hf$	0.008	0.008	0.008	–	–	0.007	0.008	0.008	0.007	0.008
$^{176}Hf/^{177}Hf$	0.282952 ± 3	0.282966 ± 9	0.282946 ± 2	–	–	0.282972 ± 2	0.282956 ± 3	0.282958 ± 7	0.282928 ± 3	0.282923 ± 2
$^{176}Hf/^{177}Hf_{(i)}$	0.28295	0.28296	0.28294	–	–	0.28297	0.28296	0.28296	0.28293	0.28292
εHf	6.36	6.86	6.14	–	–	7.06	6.49	6.58	5.52	5.34
$εHf_{(i)}$	6.35	6.85	6.12	–	–	7.06	6.49	6.57	5.52	5.32
$^{206}Pb/^{204}Pb$	19.1165 ± 6	–	19.4895 ± 16	19.2280 ± 3	19.2283 ± 2	19.461 ± 4	19.4142 ± 4	19.4018 ± 5	19.1411 ± 7	19.3952 ± 4
$^{207}Pb/^{204}Pb$	15.6367 ± 6	–	15.6443 ± 13	15.6622 ± 3	15.6346 ± 2	15.6317 ± 3	15.6443 ± 4	15.6631 ± 4	15.6393 ± 6	15.6586 ± 4
$^{208}Pb/^{204}Pb$	39.1012 ± 16	–	39.3341 ± 32	39.1994 ± 10	38.0584 ± 40	39.2580 ± 8	39.0721 ± 11	39.2131 ± 12	39.1660 ± 18	38.9782 ± 10
$^{206}Pb/^{204}Pb_{(i)}$	19.101	–	19.466	19.218	19.210	19.452	19.411	19.392	19.138	19.383
$^{207}Pb/^{204}Pb_{(i)}$	15.636	–	15.643	15.662	15.634	15.631	15.644	15.663	15.639	15.658
$^{208}Pb/^{204}Pb_{(i)}$	39.091	–	39.307	39.190	39.365	39.251	39.068	39.201	39.161	38.969

is also consistent with the positive correlations between Rb/K and Rb, Nb/Rb and Nb, Ce/K and Ce (Dalpé and Baker, 2000; Francis and Ludden, 1995) observed in MAVP lavas (El Azzouzi et al., 2010). In addition, melting experiments on natural amphibole-rich metasomatic veins at 1.5 GPa yielded alkaline melts displaying the key major and trace element features of OIB and alkaline intracontinental magmas (Pilet et al., 2008, 2010). This amphibole may have formed during a previous mantle metasomatic event caused by small-degree melts from an upwelling mantle diapir beneath the Middle Atlas. Studies of MAVP mantle xenoliths from the Bou Ibalrhatene maar (Malarkey et al., 2011; Natali et al., 2013; Raffone et al., 2009; Wittig et al., 2010a, 2010b) demonstrate the common occurrence of metasomatic amphibole- and clinopyroxene-rich spinel peridotites and pyroxenites, which are interpreted as representing fragments of the subcontinental lithospheric mantle.

5.3. Contribution of crustal components

Petrographic examination of the studied MAVP samples reveals the occasional presence of xenocrysts and xenoliths coming from the crustal basement (e.g. quartz-rich xenoliths) or from the underlying mantle. Quartz xenocrysts are very abundant (up to 5–8 modal%) in silica-saturated basalts from El Koudiate cone and flows (El Azzouzi et al., 2010). Sample MA506 collected from one of these flows is a subalkaline basalt according to Middlemost's (1975) criterions. It displays the highest SiO_2 content, La/Nb and $^{87}Sr/^{86}Sr$ ratios and the lowest Ce/Pb and εNd ratios of our dataset (Tables 1 and 2, Figs. 9a, 10a, b, c), and it seems obvious that it was contaminated by crustal materials. Various types of crustal xenoliths equilibrated under granulitic facies conditions (i.e. 850–900 °C, 0.9 ± 0.1 GPa) have been recovered in the Middle Atlas area (e.g. Moukadiri and Bouloton, 1998; Moukadiri and Pin, 1998). Although some of these xenoliths derived from igneous protoliths, most of them are metapelitic sedimentary rocks entrained by the MAVP lavas and are considered to represent refractory residues from high partial melting degrees of sedimentary sources similar to average post-Archean shales. Seismic data suggest that the lower Middle Atlas crust (located at depths ranging from 18 to 31 km) is granulitic (Ayarza et al., 2014).

A crustal flavour is less easy to detect in silica-undersatured MAVP samples. The subalkaline basalt (MA506), the alkali basalts and some basanites display higher $^{207}Pb/^{204}Pb$ and lower $^{206}Pb/^{204}Pb$ ratios than the other samples, and tend to plot away from the NHRL in Fig. 7a. Such an increase of $^{207}Pb/^{204}Pb$ ratios without concomitant elevation of $^{206}Pb/^{204}Pb$ and $^{208}Pb/^{204}Pb$ ratios is commonly ascribed to contamination processes induced by a radiogenic material such as an upper crustal component. Other geochemical tracers, such as the Ce/Pb and Hf/Sm ratios, are useful indicators to detect the contribution of crustal components mixed with the mantle magmas either in the source or during their ascent to the surface (e.g. Blichert-Toft et al., 1999; Gasperini et al., 2002). The Ce/Pb ratio may record the presence of sediments in the mantle source of alkali basalts and the Hf/Sm ratio can potentially discriminate the contributions of pelagic versus terrigenous sediments (Fig. 9a). In this diagram, our data define an elongated trend characterized by a relatively uniform Hf/Sm ratio, lower than or close to the chondritic value (0.7), whereas the Ce/Pb ratio tends to decrease from nephelinites to alkali basalts. It is worth to note the occurrence of a Ce/Pb gap between three nephelinites, characterized by significantly higher Ce/Pb ratios (N 65), and the other samples. These three samples set apart, the remaining data spread on the worldwide oceanic basalt (MORB and OIB) domain (Table 1, Fig. 9a), close to the typical HIMU value (Blichert-Toft et al., 1999; Chauvel and Blichert-Toft, 2001).

All the studied lavas yield relatively low Zr/Nb ratios, ranging from 2.08 to 4.75, with an average of 3. This is typical of primitive alkaline lavas with OIB affinities, for which low Zr/Nb ratios, ranging from 2 to 4, are commonly observed (Weaver, 1991). The continental crust is characterized by high and significantly scattered Zr/Nb ratios ranging from 8 to 14 (e.g. Rudnick and Fountain, 1995). The highest Zr/Nb ratios of our set are observed for the most evolved (i.e. the less Mg-rich) samples (Table 1), and might therefore be attributed to a contribution of crustal-derived components linked to an AFC (assimilation coupled with fractional crystallization) process. The εNd and $^{87}Sr/^{86}Sr$ versus

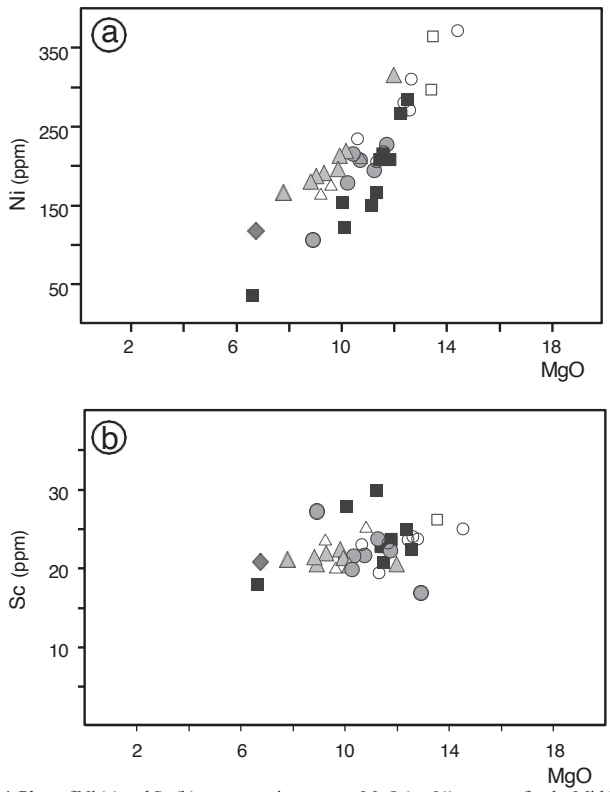

Fig. 4. Plots of Ni (a) and Sc (b) concentrations versus MgO (wt.%) contents for the Middle Atlas and Central Morocco lavas. Symbols as in Fig. 2.

SiO_2 diagrams (Fig. 10a and c) have been used to investigate the potential effects of such an AFC process. Two distinct behaviours can be distinguished. The first one, including almost all nephelinites, four basanites and only few alkali basalts defines a more or less horizontal trend parallel to the x-axes. This trend is characterized by an εNd value around ~+4.25 in Fig. 10a and by a $^{87}Sr/^{86}Sr$ of ~ 0.7032 in Fig. 10c. A second batch of samples including the nephelinite KH36, four basanites including sample KH41, five alkali basalts and the subalkaline basalt MA506 shows significantly lower εNd values (from +3.5 to +2.2) and significantly higher Sr isotopic ratios. Such a decrease of Nd isotopic composition correlated with an increase of $^{87}Sr/^{86}Sr$ (Figs. 6a, 1a and 10c) is interpreted as reflecting the contribution of a crustal component. It is worth noting that this batch includes mainly but not limited to all evolved samples.

The ortho- and paragranulite xenoliths from the Middle Atlas mountains (Le Fevre, 2002; Moukadiri and Bouloton, 1998; Moukadiri and Pin, 1998), that are believed to represent the lower crustal basement of the MAVP, have been reported in Fig. 9b and define a very large domain extending from chondritic to significantly more radiogenic $^{147}Sm/^{144}Nd$ values combined to very variable Hf/Sm ratios. Most MAVP samples exhibit Hf/Sm and $^{147}Sm/^{144}Nd$ ratios lower than the chondritic value. A few ones, especially those characterized by higher Zr/Nb ratios and lower εNd values (Fig. 10a), show Hf/Sm and $^{147}Sm/^{144}Nd$ ratios overlapping the field of ortho- and para-derived granulites. In Fig. 10b, these samples show a slightly detectable increase of both ratios. The granulites yield present-day Nd–Hf isotope signatures that extend from Bulk Earth values towards less radiogenic $^{143}Nd/^{144}Nd$ and $^{176}Hf/^{177}Hf$ isotope values (Fig. 11d). The nephelinites, basanites and alkali and sub-alkali basalts from Middle Atlas yield

$^{143}Nd/^{144}Nd$ and $^{176}Hf/^{177}Hf$ values higher than the lower crustal

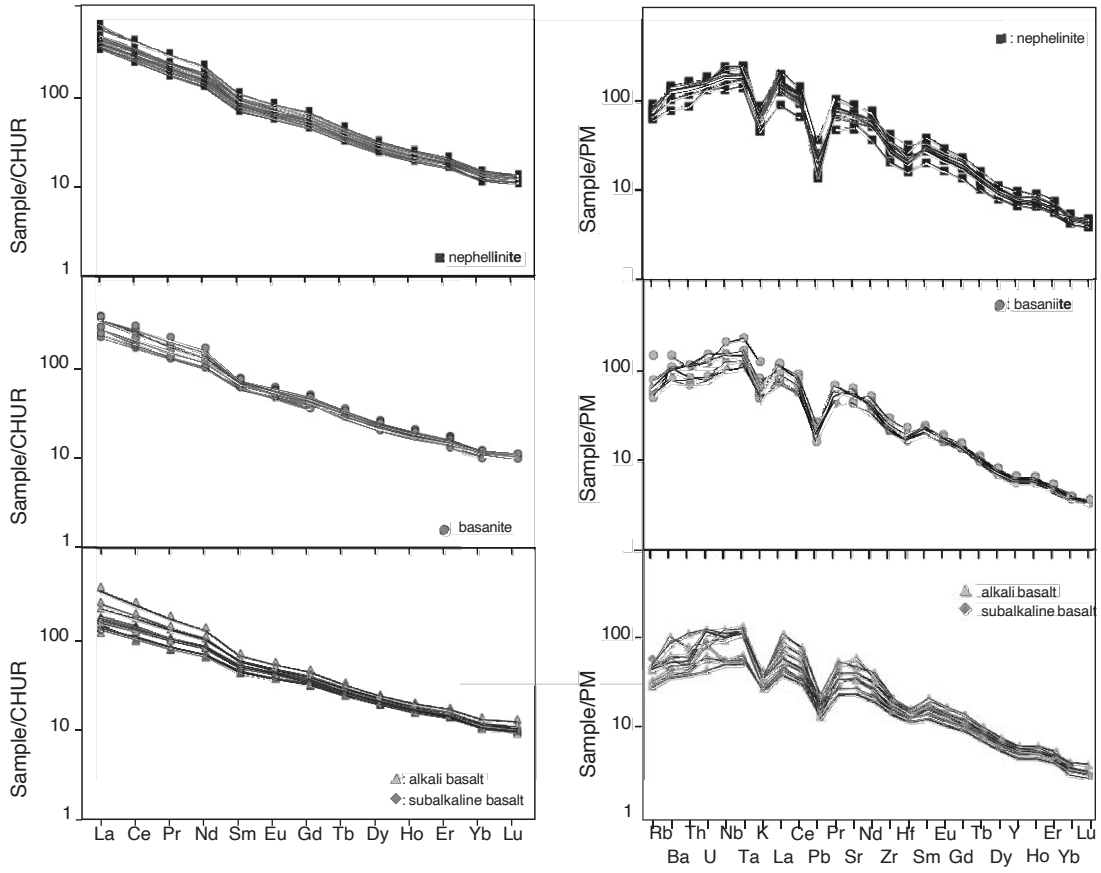

Fig. 5. Trace element patterns of Middle Atlas and Central Morocco lavas. (a) Chondrite-normalized Rare Earth elements (REE) patterns. (b) Primitive mantle-normalized elements spectra. Normalization values are from Sun and McDonough (1989). Symbols as in Fig. 2.

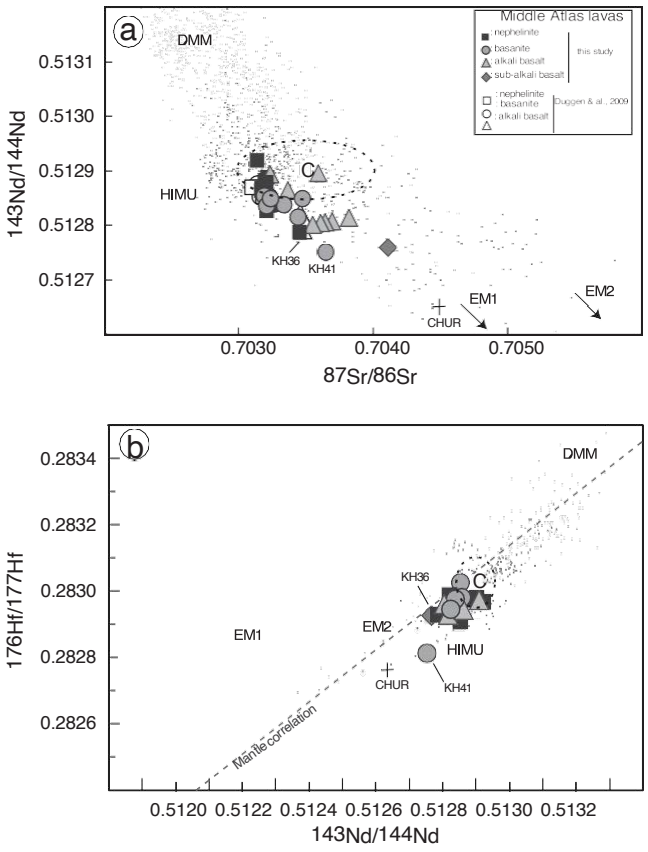

Fig. 6. Sr, Nd and Hf isotopic plots for Middle Atlas and Central Morocco lavas. a: $^{143}Nd/^{144}Nd$ versus $^{87}Sr/^{86}Sr$ diagram and b: $^{176}Hf/^{177}Hf$ versus $^{143}Nd/^{144}Nd$. The OIB (dark grey square) and MORB (pale grey square) fields are from the GEOROC database [http://georoca.mpch-mainz.gwdg.de/georoc/]. DMM, HIMU, EM-1, EM-2 and C are from Zindler and Hart (1986), Salters and White (1998) and Hanan et al. (2000). Cross: Chondritic Uniform Reservoir (CHUR) composition. Symbols as in Fig. 2.

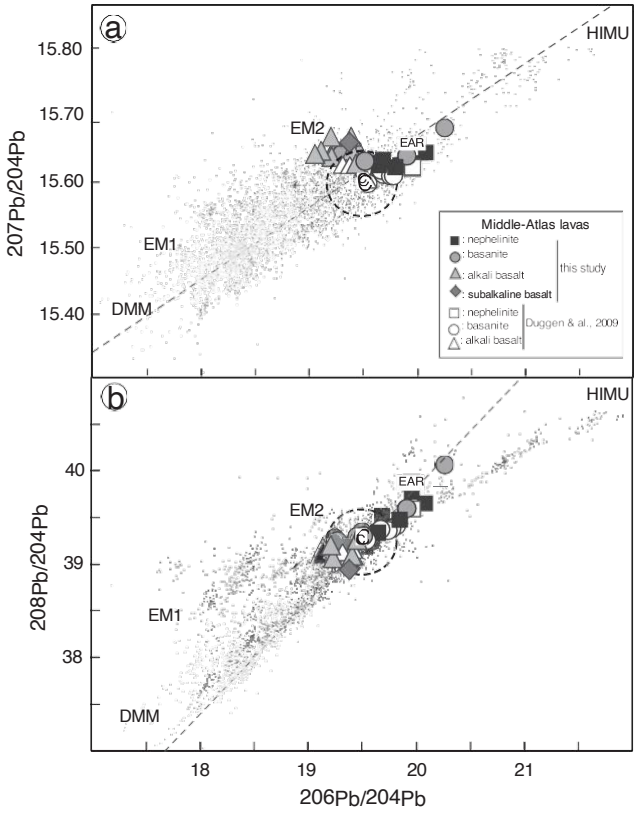

Fig. 7. Lead isotopic plots for Middle Atlas and Central Morocco lavas. a: $^{207}Pb/^{204}Pb$ versus $^{206}Pb/^{204}Pb$ diagram and b: $^{208}Pb/^{204}Pb$ versus $^{206}Pb/^{204}Pb$ diagram for the Middle Atlas basalts. The OIB (dark grey square) and MORB (pale grey circle) fields are from the GEOROC database [http://georoca.mpch-mainz.gwdg.de/georoc/]. The dashed line is the Northern Hemisphere Reference Line (NHRL). DMM, HIMU, EM-1, EM-2 and C are from Zindler and Hart (1986), Salters and White (1998) and Hanan et al. (2000). Symbols as in Fig. 2.

rocks and define a domain located in an intermediate position between DMM, HIMU and less radiogenic end-members such as MAVP crustal-derived xenoliths, EM-1 and EM-2. The Central Morocco basanite KH41 yields the lowest Nd and Hf isotopic signature of the studied lavas (very close to that of the crustal xenoliths) combined to a slightly more radiogenic $^{87}Sr/^{86}Sr$ ratio (Table 2). This feature combined with its trace element characteristics can be interpreted as indicating a strong participation of crustal materials to its genesis. The participation of a crustal component in the genesis of the MA lavas can be detected in the various studied lithologies at variable levels of contribution. It is shown that, for the various isotopic systems (Fig. 10), the samples contaminated by a crustal component display Nd and Hf isotopic ratios significantly lower than HIMU or DMM end-members and also show significantly higher $^{87}Sr/^{86}Sr$ and $^{207}Pb/^{204}Pb$ ratios. However, as no Sr or Pb isotopic data are available for the MAVP granulitic xenoliths, we cannot assess if the contaminant documented in the studied lavas corresponds or not to these granulites previously studied by Moukadiri and Pin (1998), Moukadiri and Bouloton (1998) and Le Fevre (2002).

5.4. Geochemical constraints on the source(s) of MAVP lavas

Although crustal contamination evidenced for some samples (especially alkali basalts) may have brought additional complexity, overall, the nephelinites (with the exception of sample KH36) and some of the basanites do not appear significantly contaminated by crustal materials. Therefore their trace element and isotopic signatures are likely inherited from those of their mantle sources. Mafic samples from the Middle Atlas lavas present Zr/Hf ratios ranging from 44 to 55 (Table 1), clearly higher than the chondritic value (34 following Munker et al., 2003). Clinopyroxene fractionation is commonly proposed as a suitable process explaining such behaviour (David et al., 2000). However, it is not considered as a plausible scenario for the MAVP lavas which have near-primitive compositions and show overall relatively uniform and high Sc, Co, Mn and Ni contents (Table 1 and Fig. 4). Carbonatite metasomatic events (Dupuy et al., 1992) or involvement of eclogitic components derived from a subducted oceanic crust (Pfänder et al., 2007) have also been proposed to take into account such high Zr/Hf ratios measured on some OIB and continental intraplate alkaline lavas. However, most of the neighbouring Eocene continental carbonatites from Tamazert in Central High Atlas (Bouabdellah et al., 2010) display significantly lower values, i.e. 25 (average of 18 samples) with only three carbonatites showing Zr/Hf ratios higher than 44. In addition, Nb/Ta ratios higher than the average of OIB (15.9 ± 0.6, Pfänder et al., 2007) are expected to be associated to mantle sources affected by carbonatite metasomatism (Pfänder et al., 2012). Our MAVP samples display "normal" OIB-type Nb/Ta ratios (average value 15.8, Table 1).

Previous works based on geochemistry and experimental results have suggested the presence of components derived from recycled oceanic crust in the source of some alkaline OIB magmas (e.g. Kogiso et al., 2003; Sakuyama et al., 2013). Such components would produce a significant fractionation of the Zr/Hf ratio because the extraction of slab melts during subduction produces eclogitic residues characterized by high Zr/Hf ratios due to complementary partition coefficients D_{Zr}/D_{Hf} between clinopyroxene and garnet (Klemme et al., 2002). These

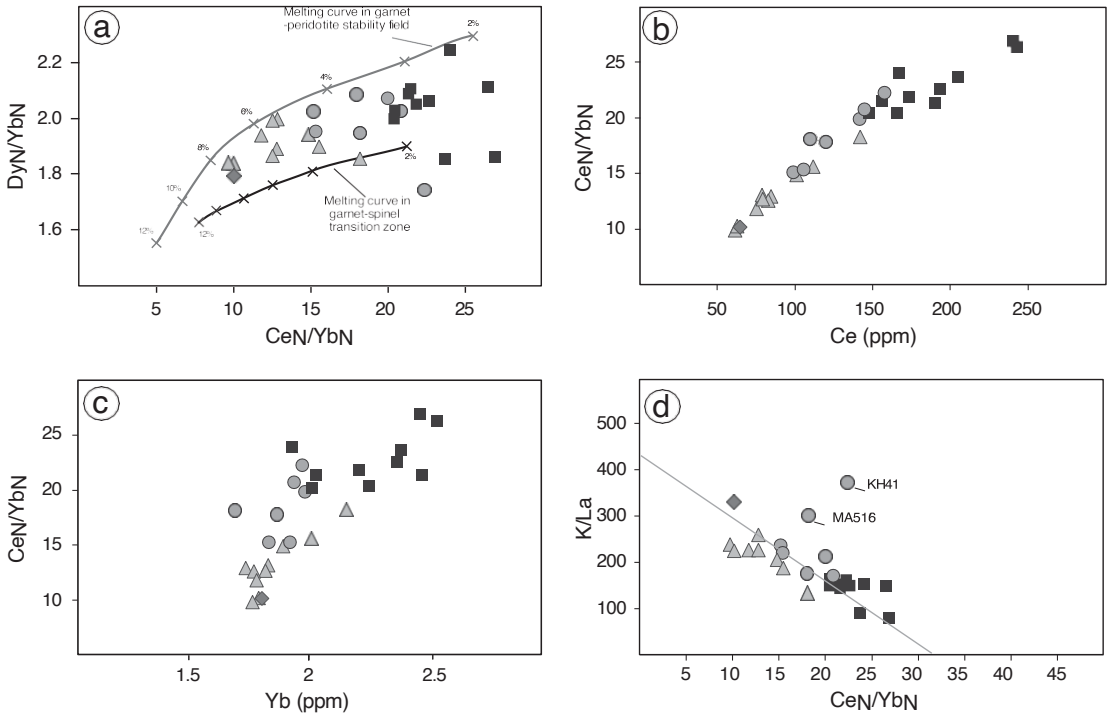

Fig. 8. Selected trace element plots for Middle Atlas and Central Morocco lavas. a: Dy_N/Yb_N versus Ce_N/Yb. The MA primary magmas were derived by melting within and/or just below the garnet–spinel transition zone. Modelled melting curves are from Haase et al. (2004). Melting curve in garnet–peridotite stability field modelled REE systematics of peridotite melting in the garnet stability field (55% olivine, 20% orthopyroxene, 21% clinopyroxene, 4% garnet). Melting curve in garnet–spinel transition zone modelled REE systematics of peridotite melting in the garnet–spinel transition zone (55% olivine, 20% orthopyroxene, 21% clinopyroxene, 1 · 5% garnet, 2 · 5% spinel). Detailed description of the REE modelling is available in Haase et al. (2004). Tick marks with numbers indicate percentages of the degree of melting; b: Ce_N/Yb_N versus Ce; c: Ce_N/Yb_N ratio versus Yb; d: K/La versus Ce_N/Yb_N. Element ratios are normalized using chondritic values from Sun and McDonough (1989). Symbols as in Fig. 2.

eclogitic residues could be incorporated later into mantle peridotites, whose melting would then impart their high Zr/Hf to any primary melts generated. Furthermore, as fractionation of the Lu/Hf ratio during mantle partial melting (e.g. between melt and clinopyroxene or garnet) is larger than that of the Sm/Nd ratio (Blundy et al., 1998), this process would result, over time, in larger time-integrated $^{176}Hf/^{177}Hf$ reservoir variations compared to $^{143}Nd/^{144}Nd$. Thus, the presence of pyroxenitic lithologies would have a strong impact on the Nd and Hf isotopic systems (Hirschmann and Stolper, 1996; Hirschmann et al., 2003).

Implication of lithospheric sources has been also suggested as an alternative model explaining the geochemical features of intraplate alkaline lavas (Hawkesworth et al., 1990; Pilet et al., 2008). Inter-element ratios such as Ce/Pb and Hf/Sm have been used to discriminate the potential contribution of lithospheric components to the genesis of MAVP lavas (Figs. 9a, 10a). Interestingly, the MAVP lavas show strong similarities with Middle Atlas mantle xenoliths and their clinopyroxenes, particularly regarding their Ce/Pb and $^{147}Sm/^{144}Nd$ ratios. However, the Hf/Sm ratios measured for MAVP lavas appear significantly higher than those determined for mantle xenoliths and associated clinopyroxenes. The most evolved lavas, i.e. alkali and subalkaline basalts, are characterized by significantly higher $^{147}Sm/^{144}Nd$ ratios combined to lower Ce/Pb ratios which could correspond to a lower continental crust contribution (Fig. 10a).

The Sr–Nd–Pb–Hf isotope compositions of the MAVP lavas exhibit a relatively large variation suggesting isotopic heterogeneities (Figs. 5, 6), that are suspected to be the result of mixing processes between various mantle components. The MAVP samples are characterized by intermediate Pb, Nd and Hf isotope ratios and define a domain largely overlapping the composition of the proposed common mantle end-member "C" (Hanan and Graham, 1996). In Fig. 5b, these samples plot slightly below the Nd–Hf mantle array and seem to scatter between "C", a HIMU-like end member (characterized by low $^{176}Hf/^{177}Hf$ for a given $^{143}Nd/^{144}Nd$ and plotting well below the mantle array) and an enriched component. Overall, MAVP lavas plot in a similar intermediate position between these different end-members in most isotopic plots (Figs. 5a, 6a, b, 9). The concept of "C" common mantle component is based on the observation of linear arrays in the Pb–Pb isotope diagrams that converge towards a central component characterized by intermediate Pb, Sr, Nd and Hf isotope signatures (Hanan and Graham, 1996). This component corresponds to oceanic crust of various ages (b 1 Ga) having incorporated a crustal component before its subduction and storage in the mantle (Hanan et al., 2000). The involvement of such an enriched "C" component has been previously detected in the Eocene Tamazert carbonatites and interpreted as indicating the presence of a Canary plume material in their source (Bouabdellah et al., 2010). Its origin has been attributed to materials residing at the top of or in a boundary layer directly above the large African superswell (Geldmacher et al., 2011; Gurenko et al., 2009).

In order to discuss in more details the origin of the MAVP lavas, previous data from alkaline magmatic suites and related lithospheric xenoliths from North Africa have been reported in isotopic diagrams (Fig. 11a, d). No noticeable isotopic difference between our samples and the 12 MAVP lavas studied by Duggen et al. (2009) has been detected in all isotopic plots, even if our sampling included a larger proportion of nephelinites. Ahaggar lavas (Allègre et al., 1981) and mantle xenoliths (Beccaluva et al., 2007a) display higher $^{143}Nd/^{144}Nd$ and $^{207}Pb/^{204}Pb$ ratios (Fig. 11a, b, c). Lavas from Canary islands, i.e. Lanzarote, La Palma and Fuerteventura, show some differences with MAVP lavas, especially regarding their higher $^{143}Nd/^{144}Nd$ ratios and slightly higher $^{176}Hf/^{177}Hf$ signature (Geldmacher et al., 2011). Compared to Eocene carbonatites from Tamazert (High Atlas), MAVP samples display distinct features such as more radiogenic $^{206}Pb/^{204}Pb$, $^{207}Pb/^{204}Pb$, $^{208}Pb/^{204}Pb$ and $^{143}Nd/^{144}Nd$ ratios combined to lower $^{87}Sr/^{86}Sr$ values and similar $^{176}Hf/^{177}Hf$ signatures (Bouabdellah et al., 2010). One striking feature is provided by the comparison between MAVP lavas and the metasomatised mantle xenoliths that they contain

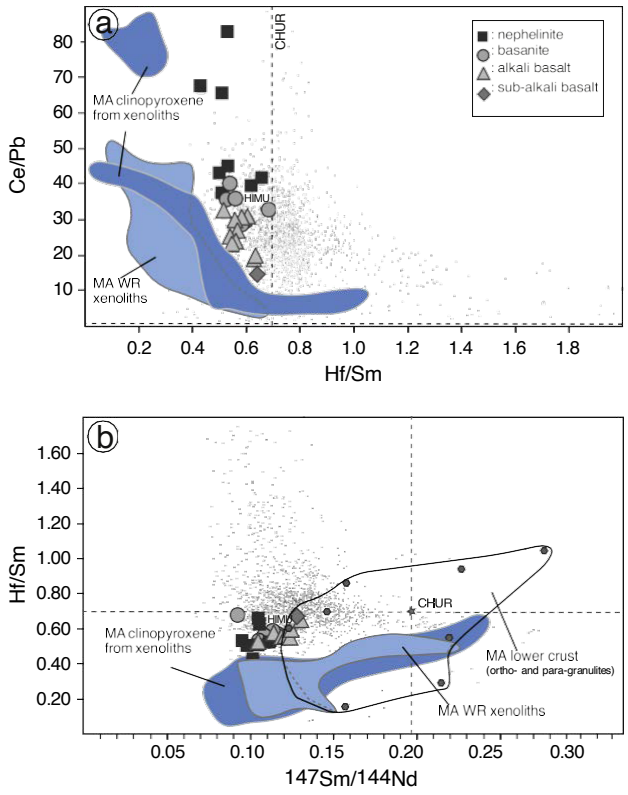

Fig. 9. Selected plots of trace element and isotopic ratios for Middle Atlas and Central Morocco lavas. a: Ce/Pb versus Hf/Sm; b: Hf/Sm versus $^{147}Sm/^{144}Nd$. The grey hexagon symbols are ortho- and paragranulite xenoliths from Middle Atlas mountains (Le Fevre, 2002; Moukadiri and Bouloton, 1998; Moukadiri and Pin, 1998). The field of MA clinopyroxene xenoliths are from Raffone et al. (2009) and Fernandez et al. (2012, in prep.) and the field of whole-rock xenoliths is from Fernandez et al. (2012, in prep.). HIMU and the mantle array are from literature sources (http://petdb.Ideo.columbia.edu/petdb/). Symbols as in Fig. 2.

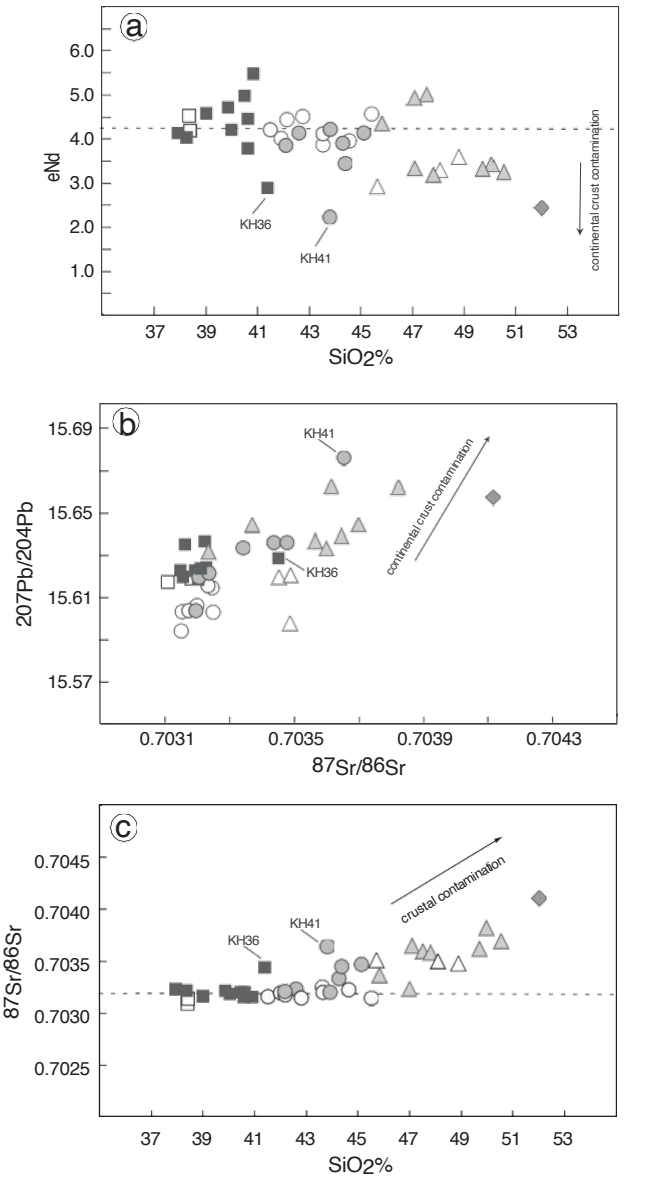

Fig. 10. a: εNd versus SiO_2 (wt.%); b: $^{207}Pb/^{204}Pb$ versus $^{87}Sr/^{86}Sr$; c: $^{87}Sr/^{86}Sr$ versus SiO_2 (wt.%). Black arrows visualize the effects of continental crust contamination. Symbols as in Fig. 2.

(Fernandez et al., 2012; Malarkey et al., 2011; Natali et al., 2013; Raffone et al., 2009; Wittig et al., 2010a, 2010b). With the exception of our most evolved samples (assumed to be contaminated by a crustal component, see Section 5.3), a remarkable similarity of isotopic signatures can be evidenced between MAVP lavas and their associated lithospheric mantle xenoliths (Fig. 11a, c). As no contamination effects of these xenoliths by their host lavas have been reported, this similarity suggests a close genetic relationship between the lavas and the associated underlying lithospheric mantle. Indeed, most uncontaminated MAVP lavas plot within the field of metasomatised lithospheric mantle xenoliths (Fig. 11c). This feature corroborates our previous assumption based on incompatible elements that an amphibole-bearing lithospheric upper mantle has played a key role in the genesis of the MAVP lavas. In addition, this genetic relationship emphasizes that it is not necessary to invoke a Quaternary asthenospheric plume to explain the HIMU flavour displayed by MAVP alkali intraplate volcanics. Indeed, the MAVP mantle xenoliths derive from a ca. 1.7 Ga old residual mantle (Natali et al., 2013; Wittig et al., 2010b) affected by a much younger (b 200 Ma) metasomatic event leading to their HIMU signature. This event involved their percolation by highly alkaline carbonate-rich melts (Natali et al., 2013) of unknown age, possibly late Cretaceous (Raffone et al., 2009) or Tertiary (ca 20 Ma according to Wittig et al., 2010a, 2010b). Although the percolating melts were chemically rather similar to MAVP nephelinites (Natali et al., 2013), their U/Pb and Th/Pb ratios are clearly distinct from those of MAVP lavas (Wittig et al., 2010a, 2010b), and their relatively low $^{3}He/^{4}He$ ratios suggest an upper mantle origin (Natali et al., 2013).

We thus propose a model in which the isotopic variations observed in MAVP lavas and, in particular, the origin of their enriched isotopic signature, are ascribed to a previous metasomatic event affecting the subcontinental lithospheric mantle during the upwelling of asthenospheric material. The presence of such an anomalous hot mantle under the Atlas Mountains has been demonstrated and considered as responsible for lithospheric delamination and thermal erosion (Bezada et al., 2013, 2014). In such a model no deep, partly recycled material, i.e. recycled sediment from a "hotspot"-type material, is invoked. However, the trace element enrichment, for example the high Zr/Hf and Hf/Sm ratios, combined with the high μ-feature ($^{238}U/^{204}Pb$) observed for all the MAVP lavas and the low $^{176}Hf/^{177}Hf$ value of some lavas (Fig. 11d), is not fully consistent with the involvement of a "normal" upper mantle material. Pilet et al. (2004) have proposed a veined stratified upper mantle with distinct compositional zones as an alternative to sediment recycling. In this model, melt percolation and vein deposition are associated with the migration of a thermal front of asthenospheric material across the lithospheric mantle (Bedini et al., 1997; Lenoir et al., 2001). Later partial melting of veins and enclosing lithospheric mantle will then form basaltic liquids. This model concurs with the estimations obtained from the trace element modelling of

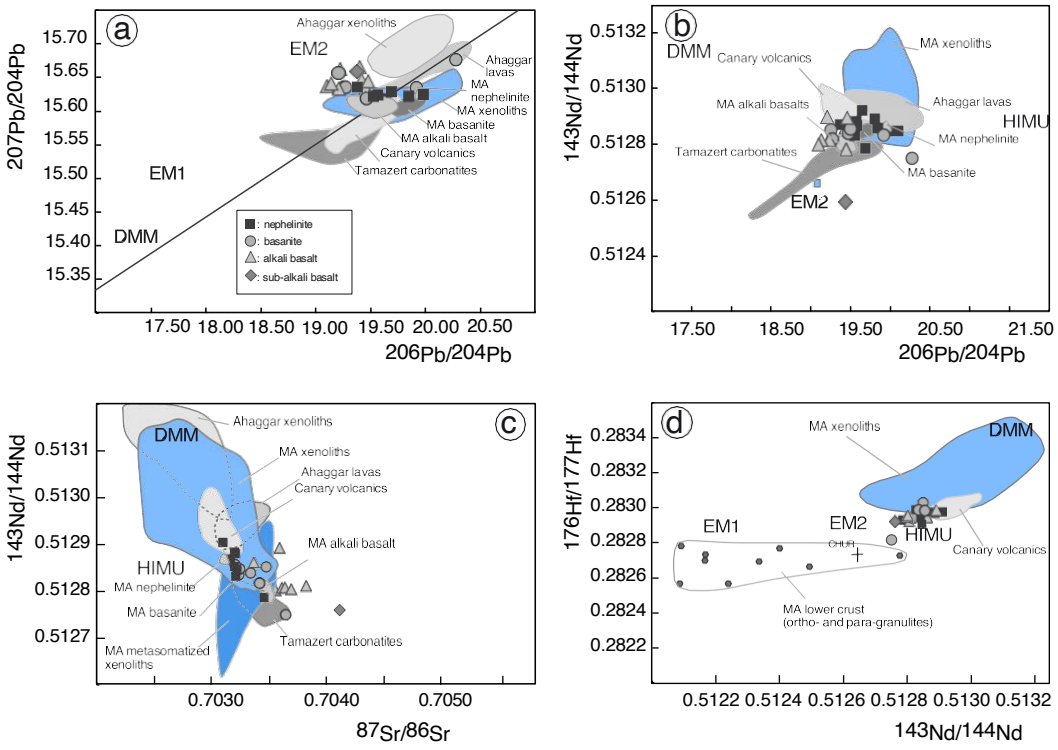

Fig. 11. Selected isotopic plots for Middle Atlas and Central Morocco lavas compared to other data sets. a: $^{206}Pb/^{204}Pb$ versus $^{207}Pb/^{204}Pb$ diagram; b: $^{143}Nd/^{144}Nd$ versus $^{206}Pb/^{204}Pb$ diagram; c: $^{143}Nd/^{144}Nd$ versus $^{87}Sr/^{86}Sr$ diagram; d $^{176}Hf/^{177}Hf$ versus $^{143}Nd/^{144}Nd$ diagram. The fields shown for comparison are those of: Ahaggar xenoliths (Beccaluva et al., 2007a); Ahaggar lavas (Allègre et al., 1981); Middle Atlas xenoliths (Wittig et al., 2010b; Raffone et al., 2009; Fernandez et al., 2012; Fernandez et al., in prep.); Middle Atlas lavas (Duggen et al., 2009); Lanzarote and La Palma volcanics (Geldmacher et al., 2011); Tamazert carbonatites (Bernard-Griffiths et al., 1991; Bouabdellah et al., 2010); and Middle Atlas lower crust ortho- and paragranulites (Moukadiri and Pin, 1998).

MAVP lava partial melting, i.e. a pressure around 2 GPa (65 km) corresponding to the spinel–garnet transition zone and to the position of the lithosphere–asthenosphere boundary beneath the MAVP (60–80 km).

5.5. Origin of MAVP lavas and comparison with other circum-Mediterranean alkaline provinces

MAVP lavas, as well as their mantle xenoliths, display the enriched HIMU imprint typical of circum-Mediterranean alkaline lavas (Hoernle et al., 1995; Lustrino and Wilson, 2007; Piromallo et al., 2008; Wilson and Downes, 2006). A central question is whether or not this trace element and isotopic signature is due to the partial melting of the hot asthenospheric mantle. This mantle might occur as either "genuine" deep-seated plumes or superplumes, "splash plumes" or "hot small fingers" commonly envisioned for the origin of OIB or continental intraplate alkali provinces (Xie and Tackley, 2004). However, Neogene alkaline magmatism in Morocco emplaced rather small volumes of lavas (less than 50 km^3, including 20 km^3 for the MAVP, according to Frizon de Lamotte et al., 2008) and the corresponding SW–NE trend of volcanic centers (Fig. 1, inset) does not show gradual age progression. These features are hardly consistent with a "conventional" hotspot activity involving a deep-rooted mantle plume located beneath this region (Berger et al., 2010; Bouabdellah et al., 2010; El Azzouzi et al., 2010; Frizon de Lamotte et al., 2008; Lustrino and Wilson, 2007; Missenard and Cadoux, 2012). In addition, recent tomographic data (Bezada et al., 2014) suggest the occurrence of a delaminated "cold" lithospheric body at ca. 400 km beneath the Middle Atlas and therefore do not support the hypothesis of a deep-rooted plume. This body is overlain by a corridor of hot mantle extending from lithospheric (N 50 km) to asthenospheric (90 km) depths below the thinned lithospheric areas, and to 160 km beneath the MAVP (Bezada et al., 2014). The origin of this hot mantle and of the corresponding lithospheric thinning have been attributed either to the flow around the retreating Alboran slab of mantle material (Duggen et al., 2005), possibly emanating from the Canary mantle plume (Bezada et al., 2013, 2014; Duggen et al., 2009); or to edge-driven convection around the West African craton (Missenard and Cadoux, 2012). In the last model, upwelling of the asthenosphere underneath the Middle Atlas area could be the result of activation of convective cells (Facenna and Becker, 2010), possibly driven by edge effects (King and Anderson, 1998). Such edge-driven convection can induce thermal erosion of the base of the continental lithosphere and thus can explain the location and elongated geometry of the Atlas lithosphere thinning identified by geophysical studies.

Does a chemical contribution of this hot asthenospheric mantle explain the enriched HIMU-type imprint of MAVP lavas, or alternatively is this mantle only responsible for the conductive heating and partial melting of the base of the overlying thinned lithosphere? An important argument is that relatively old Moroccan lavas share the isotopic signature described above: it is the case of the oldest nephelinites from this study (16 Ma), the Eocene (44–35 Ma) Tamazert carbonatites (Bernard-Griffiths et al., 1991; Bouabdellah et al., 2010) and the Early Tertiary (67–37 Ma) Taourirt lamprophyres and associated carbonatites (Wagner et al., 2003). If the HIMU imprint was carried by an asthenospheric mantle flux from the Canary plume (Duggen et al., 2009), then this flux was operating since 45 Ma for Tamazert (Bouabdellah et al., 2010) or even earlier for Taourirt, and thus probably since the early stages of the Canary hot spot activity (Anguita and Hernan, 2000). Alternatively, if the isotopic imprint of MAVP lavas was inherited from the underlying lithospheric mantle metasomatised during the Late Cretaceous as suggested by xenolith data (Raffone et al., 2009), then Tertiary or Quaternary geodynamic events (regional extension, mantle flow around retreating slabs or African craton boundary, e.g. Boschi et al., 2010) were able to trigger hot mantle flux and upwelling, that induced partial melting of the base of the African lithosphere. The latter hypothesis is consistent with the obvious geochemical similarities

between MAVP lavas and their lithospheric mantle xenoliths, as well as with the fit of their depth of origin (Section 5.2) with that of the lithosphere–asthenosphere boundary beneath the Middle Atlas (60–80 km).

The case of MAVP and its Moroccan neighbours is rather representative of that of a number of Tertiary and Quaternary circum-Mediterranean alkaline provinces, which is characterized by intermittent activity over 50 Ma or even more (e.g. Languedoc, Dautria et al., 2010), small volumes of erupted sodic lavas and an overall HIMU flavour (Lustrino and Wilson, 2007). Most of these suites contain metasomatised lithospheric mantle xenoliths which have interacted with alkaline melts under mantle conditions (Ackerman et al., 2013; Downes, 2001). The geochemical features of these alkaline lavas have been ascribed to the melting of an European Asthenospheric Reservoir (EAR, Cebria and Wilson, 1995) or Low Velocity Composition reservoir (LVC, Hoernle et al., 1995), or to that of the top of the asthenospheric mantle, with a variable contribution from the base of the lithosphere (Wilson and Downes, 2006). A mixed lithospheric/asthenospheric origin was proposed for Vogelsberg and Westerwald, Germany (Bogaard and Wörner, 2003; Haase et al., 2004). However, a mostly or purely lithospheric origin seems more plausible in many cases (Lustrino and Wilson, 2007; Piromallo et al., 2008), e. g. the Adriatic Province (Beccaluva et al., 2007b) or Languedoc (Dautria et al., 2010). Piromallo et al. (2008) have ascribed the origin of these HIMU-like volcanic provinces to a late Cretaceous contamination episode of the Euro-Mediterranean mantle by melts from the Central Atlantic Plume, the ancestor of the Canary plume (Oyarzun et al., 1997). The resulting metasomatised mantle migrated towards NE as a part of the Eurasian and African plates until its present-day position beneath the alkaline volcanic centers of northwestern Africa and western Europe. This model accounts especially well for the geochemical features shared by MAVP and Canary lavas (Duggen et al., 2009), because of their relative proximity within the huge circum-Mediterranean region.

HIMU-like enriched isotopic signatures have also been identified in Tertiary and Quaternary alkali intra-plate lavas (and their mantle xenoliths) from areas located far away from the western Mediterranean, such as Ahaggar, Algeria (Beccaluva et al, 2007a; Liégeois et al., 2005), NW Lybia (Beccaluva et al., 2008), Sudan and Egypt (Lucassen et al., 2008), Israel (Weinstein et al., 2006), Syria, Yemen and Saudi Arabia (Baker et al., 1998; Bertrand et al., 2003; Chazot and Bertrand, 1993). Their geochemical features, although variable from one occurrence to another, have been interpreted as indicating a major involvement of "metasomes" from the subcontinental lithospheric mantle (Rooney et al., 2014). The mantle beneath Ahaggar and NW Lybia could have been exposed to contamination by the Cretaceous Central Atlantic Plume melts according to Piromallo et al.'s (2008) reconstructions. However, this was not the case for that of the remaining areas, which could have interacted with other deep-rooted African/Arabian plumes also displaying a HIMU-like flavour (Pik et al., 2006). In short, the HIMU-like imprint of the subcontinental lithospheric mantle was acquired through its interaction with alkaline (or sometimes carbonatitic) melts derived from the heads of long-lived plumes such as the Central Atlantic/Canary plume (Oyarzun et al., 1997; Piromallo et al., 2008) or the Afar plume (Furman et al., 2006). Then, upwelling of hot asthenospheric mantle controlled by various tectonic events (intraplate extension, rifting, slab retreat, lithospheric delamination; e.g. Carminati et al., 2012) caused the partial melting of the base of this metasomatised lithospheric mantle, and the subsequent episodic emplacement of small amounts of sodic alkaline lavas such as those of Middle Atlas and Central Morocco volcanic provinces.

6. Conclusions

1. Mafic lavas from the Middle Atlas and Central Morocco volcanic provinces include Miocene nephelinites (16.2–5.9 Ma) and Pliocene–Quaternary (3.9–0.6 Ma) nephelinites, basanites, alkali basalts and subalkaline basalts. Most of them represent near-primary magmas which experienced minor fractionation/accumulation processes involving olivine and diopside phenocrysts. Subalkaline basalt MA506 contains quartz xenocrysts and displays the highest SiO_2 contents, La/Nb and $^{87}Sr/^{86}Sr$ ratios of our dataset, which emphasize its contamination by crustal materials. Similar processes of contamination by an enriched component have been also evidenced in some basanites, and alkali basalts, which exhibit significantly higher $^{207}Pb/^{204}Pb$, $^{87}Sr/^{86}Sr$ and Zr/Nb ratios and lower εNd and εHf than the other samples. We attribute these features to their contamination by lower crustal granulites during an open fractionation process.
2. The progressive enrichment in incompatible elements observed from alkali basalts to nephelinites is consistent with decreasing partial melting degrees (from 7–8 to 2%) of an enriched mantle source located in the garnet–spinel transition zone (1.8–2.2 GPa). The strong negative spikes observed for K in multielement patterns suggest that this source contained a residual pargasitic amphibole, which experienced dehydration melting under pressures slightly lower than 2 GPa (Niida and Green, 1999). These features suggest that melting occurred under pressures around 2 GPa. The corresponding depth (65 km) fits that of the lithosphere–asthenosphere boundary beneath the Middle Atlas (60–80 km). Abundant metasomatic amphibole- and clinopyroxene-rich peridotites and pyroxenites carried by Middle Atlas lavas may represent an analog of their source.
3. The trace element and isotopic Sr–Nd–Pb–Hf signature of the uncontaminated lavas is intermediate between those of "C", HIMU and an enriched mantle. Its strong similarities with that of Middle Atlas lithospheric mantle xenoliths and their clinopyroxenes, particularly regarding their Ce/Pb and $^{147}Sm/^{144}Nd$ ratios, suggest a genetic relationship. Low degrees of melting of amphibole-bearing ultramafic materials equivalent to these xenoliths account for most of the geochemical features of the studied lavas. It is therefore not necessary to postulate the contribution of "fresh" asthenospheric mantle to their source.
4. The Middle Atlas and Central Morocco volcanic provinces share the characteristics of a number of circum-Mediterranean alkaline suites from western Europe and northwestern Africa: intermittent activity, small volumes of erupted sodic lavas of HIMU-like flavour, and common occurrence of metasomatised amphibole-bearing mantle xenoliths (Lustrino and Wilson, 2007). These features have been attributed to the melting of the base of a veined lithospheric mantle metasomatised during the late Cretaceous by alkaline melts originating from the Central Atlantic plume, the ancestor of the Canary plume (Piromallo et al., 2008). In the specific case of Middle Atlas, this interpretation is supported by (i) the late Cretaceous or early Tertiary age of the metasomatic event that affected the lithospheric mantle xenoliths (Raffone et al., 2009), (ii) the isotopic and trace element signature that the latter share with their host lavas, and (iii) the origin of these lavas at depths consistent with the base of the Middle Atlas thinned lithosphere. Melting was probably triggered by the flux of hot mantle within a regional SW–NE sub-lithospheric channel, in response to either the Alboran slab retreat (Duggen et al., 2009) or edge-driven convection around the West African craton (Missenard and Cadoux, 2012).

Acknowledgments

We thank N. Youbi, F. Kharbouch, M.-F. Maury and A. Piqué for their contribution to sampling and field studies in the Middle Atlas. We are grateful to B. Galland for her help on the management of the isotope laboratory of Montpellier. We also thank P. Télouk (ENS Lyon) for his help during MC–ICP-MS analyses at the national facility service. Comments by Hilary Downes, Andrew Kerr and an anonymous reviewer helped us considerably to improve the discussion and the overall presentation of the manuscript.

References

Ackerman, L., Spacek, P., Magna, T., Ulrych, J., Svojtka, M., Hegner, E., Balogh, K., 2013. Alkaline and carbonate-rich melt metasomatism and melting of subcontinental lithospheric mantle: evidence from mantle xenoliths, NE Bavaria, Bohemian Massif. Journal of Petrology 54, 2597–2633.

Allègre, C.J., Treuil, M., Minster, J.F., Minster, B., Albarède, F., 1977. Systematic use of trace element in igneous processes. Part I: Fractional crystallization processes in volcanic suites. Contributions to Mineralogy and Petrology 60, 57–75.

Allègre, C.J.,Dupré, B.,Lambret, B.,Richard, P., 1981. The subcontinental versus suboceanic debate. I. Lead–neodymium–strontium isotopes in primary alkali basalts from a shield area: the Ahaggar volcanic suite. Earth and Planetary Science Letters 52, 85–92.

Anguita, F.,Hernan, F., 2000. The Canary Islands origin: a unifying model. Journal of Volcanology and Geothermal Research 103, 1–26.

Ayarza, P., Carbonell, R., Teixell, A., Palomeras, I., Marti, D., Kchikach, A., Harnafi, M., Levander, A., Gallart, J., Arboleya, M.L., Alcade, J., Fernandez, M., Charroud, M., Amrhar, M., 2014. Crustal thickness and velocity structure across the Moroccan Atlas from long offset wide-angle reflection seismic data: the SIMA experiment. Geochemistry, Geophysics, Geosystems. http://dx.doi.org/10.1002/2013GC005164.

Baker, J., Chazot, G., Menzies, M., Thirlwall, M., 1998. Metasomatism of the shallow mantle beneath Yemen by the afar plume — implications for mantle plumes, flood volcanism, and intraplate volcanism. Geology 26, 431–434.

Barrat, J.A., Yamaguchi, A., Greenwood, R.C., Bohn, M., Cotten, J., Benoit, M., Franchi, I.A., 2007. The Stannern trend eucrites: contamination of main group eucritic magmas by crustal partial melts. Geochimica et Cosmochimica Acta 71, 4108–4124.

Barruol, G., Granet, M., 2002. A Tertiary asthenospheric flow beneath the southern French Massif Central indicated by upper mantle seismic anisotropy and related to the west Mediterranean extension. Earth and Planetary Science Letters 202, 31–47.

Barruol, G., Deschamps, A., Coutant, O., 2004. Mapping upper mantle anisotropy beneath SE France by SKS splitting indicates Neogene asthenospheric flow induced by Apenninic slab roll-back and deflected by the deep Alpine roots. Tectonophysics 394, 125–138.

Beccaluva, L.,Azzouni-Sekkal, A., Benhallou, A.,Bianchini, G.,Ellam, R.M.,Marzola, M.,Sian, F., Stuart, F.M., 2007a. Intracratonic asthenosphere upwelling and lithosphere rejuvenation beneath the Hoggar swell (Algeria): evidence from HIMU metasomatised lherzolite mantle xenoliths. Earth and Planetary Science Letters 260, 482–494.

Beccaluva, L., Bianchini, G., Bonadiman, C., Coltorti, M., Milani, L., Salvini, L., Siena, F., Tassarini, R., 2007b. Intraplate lithospheric and sublithospheric components in the Adriatic domain: nephelinite to tholeiite magma generation in the Paleogene Veneto volcanic province, Southern Alps. In: Beccaluva, L., Bianchini, G., Wilson, M. (Eds.), Cenozoic Volcanism in the Mediterranean Area. Geological Society of America Special Paper, 418, pp. 131–152.

Beccaluva, L., Bianchini, G., Ellam, R.M., Marzola, M., Oun, K.M., Siena, F., Stuart, F.M., 2008. The role of HIMU metasomatic components in the North African lithospheric mantle: petrological evidence from the Gharyan lherzolite xenoliths, NW Lybia. In: Coltorti, M., Grégoire, M. (Eds.), Metasomatism in Oceanic and Continental Lithospheric Mantle. Geological Society, London, Special Publication, 293, pp. 253–277.

Bedini, R.M.,Bodinier, J.-L.,Dautria, J.-M.,Morten, L., 1997. Evolution of LILE-enriched small melt fractions in the lithospheric mantle: a case study from the East African Rift. Earth and Planetary Science Letters 153, 67–83.

Bertrand, H.,Chazot, G., Blichert-Toft, J., Thoral, S., 2003. Implications of widespread high-μ volcanism on the Arabian Plate for Afar mantle plume and lithosphere composition. Chemical Geology 198, 47–61.

Berger, J., Liégeois, J.-P., Ennih, N., Bonin, B., 2010. Flow of Canary mantle plume material through a subcontinental lithospheric corridor beneath Africa to the Mediterranean: comment. Geology 38, e202. http://dx.doi.org/10.1130/G30516C.1.

Bernard-Griffiths, J., Fourcade, S., Dupuy, C., 1991. Isotopic study, Sr, Nd, O and C of lamprophyres and associated dykes from Tamazert, Morocco: crustal contamination process and source characteristics. Earth and Planetary Science Letters 103, 190–199.

Bezada, M.J., Humphreys, E.D., Toomey, D.R., Harnafi, M., Davila, J.M., Gallart, J., 2013. Evidence for slab rollback in westernmost Mediterranean from improved upper mantle imaging. Earth and Planetary Science Letters 368, 51–60.

Bezada, M.J.,Humphreys, E.D.,Davila, J.M.,Carbonell, R.,Harnafi, M.,Palomeras, I.,Levander, A., 2014. Piecewise delamination of Moroccan lithosphere from beneath the Atlas Mountains. Geochemistry, Geophysics, Geosystems. http://dx.doi.org/10.1002/2013GC005059.

Blichert-Toft, J.,Albarède, F., 1997. The Lu–Hf isotope geochemistry of chondrites and the evolution of the mantle–crust system. Earth and Planetary Science Letters 148, 243–258.

Blichert-Toft, J., Frey, F.A., Albarède, F., 1999. Hf isotope evidence for pelagic sediments in the source of Hawaiian basalts. Science 285, 879–882.

Blundy, J.D., Robinson, J.A.C., Wood, B.J., 1998. Heavy REE are compatible in clinopyroxene on the spinel lherzolite solidus. Earth and Planetary Science Letters 160, 493–504.

Bogaard, P.J.F.,Wörner, G., 2003. Petrogenesis of basanitic to tholeiitic volcanic rocks from the Miocene Vogelsberg, Central Germany. Journal of Petrology 44, 569–602.

Boschi, L.,Facenna, C.,Becker, T.W., 2010. Mantle structure and dynamic topography in the Mediterranean Basin. Geophysical Research Letters 37, L20303. http://dx.doi.org/10.129/2010GL045001.

Bouabdellah, M.,Hoernle, K., Kchit, A., Duggen, S., Hauff, F., Klügel, A., Lowry, D.E.,Beaudoin, G., 2010. Petrogenesis of the Eocene Tamazert continental carbonatites (Central High Atlas, Morocco): implications for a common source for the Tamazert and Canary and Cape Verde Island carbonatites. Journal of Petrology 51, 1655–1686.

Carminati, E., Lustrino, M., Doglioni, C., 2012. Geodynamic evolution of the Central and Western Mediterranean: tectonics vs. igneous petrology constraints. Tectonophysics 579, 173–192.

Cebria, J.M., Wilson, M., 1995. Cenozoic mafic magmatism in Western/Central Europe: a common European asthenospheric reservoir. Terra Nova 7, 162 (162 Abstract Supplement 7).

Chauvel, C., Blichert-Toft, J., 2001. A hafnium isotope and trace element perspective on melting of the depleted mantle. Earth and Planetary Science Letters 190, 137–151.

Chauvel, C., Jahn, B.M., 1984. Nd–Sr isotope and REE geochemistry of alkali basalts from the Massif central, France. Geochimica et Cosmochimica Acta 48, 93–110.

Chazot, G., Bertrand, H., 1993. Mantle sources and magma–continental crust interactions during early Red Sea-Gulf of Aden rifting in Southern Yemen: elemental and Sr, Nd, Pb isotope evidence. Journal of Geophysical Research 98, 1819–1835.

Class, C., Goldstein, S.L., 1997. Plume–lithosphere interactions in the ocean basins: constraints from the source mineralogy. Earth and Planetary Science Letters 150, 245–260.

Connelly, J.N.,Ulfbeck, D.G.,Thrane, K.,Bizzarro, M.,Housh, T., 2006. A method for purifying Lu and Hf for analyses by MC–ICP-MS using TODGA resin. Chemical Geology 233, 126–136.

Cotten, J.,Le Dez, A.,Bau, M.,Caroff, M.,Maury, R.C.,Dulski, P.,Fourcade, S.,Bohn, M.,Brousse, R., 1995. Origin of anomalous rare-earth element and yttrium enrichments in subaerially exposed basalts: evidence from French Polynesia. Chemical Geology 119, 115–138.

Coulon, C., Megartsi, M., Fourcade, S., Maury, R.C., Bellon, H., Louni-Hacini, A., Cotten, J., 2002. Postcollisional transition from calc-alkali to alkali volcanism during the Neogene in Oranie (Algeria): magmatic expression of a slab breakoff. Lithos 62, 87–110.

Dalpé, C., Baker, D.R., 2000. Experimental investigation of large-ion-lithophile-element-, high-field-strength-element- and rare-earth-element-partitioning between calcic amphibole and basaltic melt: the effects of pressure and oxygen fugacity. Contributions to Mineralogy and Petrology 140, 233–250.

Dautria, J.-M., Liotard, J.-M., Bosch, D., Alard, O., 2010. 160 Ma of sporadic basaltic activity on the Languedoc volcanic line (Southern France): a peculiar case of lithosphere–asthenosphere interplay. Lithos 120, 202–222.

David, K., Schiano, P., Allègre, C.J., 2000. Assessment of the Zr/Hf fractionation in oceanic basalts and continental materials during petrogenetic processes. Earth and Planetary Science Letters 178, 285–301.

Davies, J.H., Bunge, H.P., 2006. Are splash plumes the origin of minor hotspots? Geology 34, 349–352.

Downes, H., 2001. Formation and modification of the shallow sub-continental lithospheric mantle: a review of geochemical evidence from ultramafic xenoliths suites and tectonically emplaced ultramafic massifs of Western and Central Europe. Journal of Petrology 42, 233–250.

Duggen, S., Hoernle, K., van den Bogaard, P., Garbe-Schönberg, A., 2005. Post-collisional transition from subduction to intraplate-type magmatism in the westernmost Mediterranean: evidence for continental-edge delamination of subcontinental lithosphere. Journal of Petrology 46, 1155–1201.

Duggen, S., Hoernle, K.A.,Hauff, F., Klügel, A., Bouabdellah, M., Thirlwall, M.F., 2009. Flow of Canary mantle plume material through a subcontinental lithospheric corridor beneath Africa to the Mediterranean. Geology 37, 283–286.

Dupuy, C., Liotard, J.-M., Dostal, J., 1992. Zr/Hf fractionation in intraplate basaltic rocks: carbonate metasomatism in the mantle source. Geochimica et Cosmochimica Acta 56, 2417–2423.

El Azzouzi, M., 2002. Volcanisme alcalin et calco-alcalin and contexte post-collision continentale: exemple du Maroc(Thèse Doctorat d'Etat) University Mohammed V-Agdal, Rabat (289 pp.).

El Azzouzi, M., Bernard-Griffiths, J., Bellon, H., Maury, R.C., Piqué, A., Fourcade, S., Cotten, J., Hernandez, J., 1999. Evolution des sources du volcanisme marocain au cours du Néogène. Comptes Rendus de l'Académie des Sciences, Paris, série II 329, 95–102.

El Azzouzi, M., Maury, R.C., Bellon, H., Youbi, N., Cotten, J., Kharbouch, F., 2010. Petrology and K–Ar chronology of the Neogene–Quaternary Middle Atlas basaltic province, Morocco. Bulletin de la Societe Geologique de France 181, 243–257.

Facenna, C., Becker, T.W., 2010. Shaping mobile belts by small-scale convection. Nature 465, 602–605.

Fernandez, L.,Elmessbahi, H.,Bosch, D.,Bodinier, J.L.,Dautria, J.M.,Verdoux, P., 2012. Trace elements and isotopes from Middle Atlas xenoliths (Morocco): lithosphere–asthenosphere interaction processes. European Mineralogical Congress, Francfort (Allemagne), 2–6 September.

Forte, A.,Quéré, S.,Moucha, R.,Simmons, N.A.,Grand, S.P.,Mitrovica, J.X.,Rowley, D.R., 2010. Joint seismic–geodynamic–mineral physical modelling of African geodynamics: a reconciliation of deep-mantle convection with surface geophysical constraints. Earth and Planetary Science Letters 295, 329–341.

Francis, D.,Ludden, J., 1995. The signature of amphibole in mafic alkali lavas, a study in the Northern Canadian Cordillera. Journal of Petrology 36, 1171–1191.

Frey, F.A.,Green, D.H., Roy, D.S., 1978. Integrated models of basalt petrogenesis: a study of quartz-tholeiites to olivine-melilites from south-eastern Australia utilizing geochemical and experimental petrological data. Journal of Petrology 19, 463–513.

Frizon de Lamotte, D.,Zizi, M.,Missenard, Y.,Hafid, M.,El Azzouzi, M.,Maury, R.C.,Charrière, A., Taki, Z., Benammi, M., Michard, A., 2008. Chapter 4: The Atlas System. In: Michard, A., Saddiqi, O., Chalouan, A., Frizon de Lamotte, D. (Eds.), Continental Evolution: The Geology of Morocco. Structure, Stratigraphy and Tectonics of the Africa–Atlantic–Mediterranean Triple Junction. Lecture Notes in Earth Sciences, 116. Springer-Verlag, Berlin, Heidelberg, pp. 133–202.

Fullea, J.,Fernàndez, M.,Alfonso, J.C.,Vergés, J.,Zeyen, H., 2010. The structure and evolution of the lithosphere–asthenosphere boundary beneath the Atlantic–Mediterranean Transition Region. Lithos 120, 74–95.

Furman, T., 1995. Melting of metasomatized subcontinental lithosphere: undersaturated mafic lavas from Rungwe, Tanzania. Contributions to Mineralogy and Petrology 122, 97–115.

Furman, T.,Bryce, J.,Rooney, T.,Hana, B.,Yirgu, G.,Ayalew, D., 2006. Heads and tails: 30 million years of the Afar plume. In: Yirgu, G., Ebinger, C.J., Maguire, P.K.H. (Eds.), The Afar Volcanic Province within the East African Rift System. Geological Society of London, Special Publication, 259, pp. 95–119.

Gasperini, D.,Blichert-Toft, J.,Bosch, D.,Del Moro, A.,Macera, P.,Albarède, F., 2002. Upwelling of deep mantle material into a plate window: evidence from the geochemistry of Italian basaltic volcanics. Journal of Geophysical Research 107, 2367.

Geldmacher, J., Hoernle, K., Hanan, B.B., Blichert-Toft, J., Hauff, F., Gill, J.B., 2011. Hafnium isotopic variations in East Atlantic intraplate volcanism. Contributions to Mineralogy and Petrology 162, 21–36.

Goes, S., Spakman, W., Bijwaard, H., 1999. A lower mantle source for Central European volcanism. Science 286, 1928–1931.

Granet, M., Wilson, M., Achauer, U., 1995. Imaging a mantle plume beneath the French Massif Central. Earth and Planetary Science Letters 136, 281–296.

Gurenko, A.A., Sobolev, A.V., Hoernle, K.A., Hauff, F., Schmincke, H.-U., 2009. Enriched, HIMU-type peridotite and depleted recycled pyroxenite in the Canary plume: a mixed-up mantle. Earth and Planetary Science Letters 277, 514–524.

Haase, K.M., Goldschmidt, B., Garbe-Schönberg, C.-D., 2004. Petrogenesis of Tertiary continental intra-plate lavas from the Westerwald region, Germany. Journal of Petrology 45, 883–905.

Hanan, B.B., Graham, D.W., 1996. Lead and helium isotope evidence from oceanic basalts for a common deep source of mantle plumes. Science 272, 991–995.

Hanan, B.B., Blichert-Toft, J., Kingsley, R., Schilling, J.G., 2000. Depleted Iceland mantle plume geochemical signature: artifact of multi-component mixing? Geochemistry, Geophysics, Geosystems 1 (Paper number 1999GC000009).

Harmand, C., Cantagrel, J.-C., 1984. Le volcanisme alcalin Tertiaire et Quaternaire du Moyen Atlas, Maroc): chronologie K/Ar et cadre géodynamique. Journal of African Earth Sciences 2, 51–55.

Hawkesworth, C.J., Kempton, P.D., Rogers, N.W., Ellam, R.M., Van Calsteren, P.W., 1990. Continental mantle lithosphere, and shallow level enrichment in the Earth's mantle. Earth and Planetary Science Letters 96, 256–268.

Hernandez, J., Bellon, H., 1985. Chronologie K–Ar du volcanisme miocène du Rif oriental, Maroc: implication tectoniques et magmatologiques. Revue de Géologie Dynamique et de Géographie Physique 26 (2), 85–94.

Hirschmann, M.M., Stolper, E.M., 1996. A possible role for garnet pyroxenite in the origin of the "garnet signature" in MORB. Contributions to Mineralogy and Petrology 124, 185–208.

Hirschmann, M.M.,Kogiso, T., Baker, M.B., Stolper, E.E.M., 2003. Alkalic magmas generated by partial melting of gernet pyroxenite. Geology 31, 481–484.

Hoernle, K., Zhang, Y.S., Graham, D., 1995. Seismic and geochemical evidence for large-scale mantle upwelling beneath the eastern Atlantic and western and central Europe. Nature 374, 34–39.

Jacobsen, S.B., Wasserburg, G.J., 1980. Sm–Nd isotopic evolution of chondrites. Earth and Planetary Science Letters 50, 139–155.

King, S.D., Anderson, D.L., 1998. Edge-driven convection. Earth and Planetary Science Letters 160, 289–296.

Klemme, S., O'Neill, H.St.C., 2000. The near-solidus transition from garnet lherzolite to spinel lherzolite. Contributions to Mineralogy and Petrology 138, 237–248.

Klemme, S.,Blundy, J.D., Wood, B.J., 2002. Experimental constraints on major and trace element partitioning during partial melting of eclogite. Geochimica et Cosmochimica Acta 66, 3109–3123.

Kogiso, T., Hirschmann, M.M., Frost, D.J., 2003. High-pressure partial melting of garnet pyroxenite: possible mafic lithologies in the source of ocean island basalts. Earth and Planetary Science Letters 216, 603–617.

Langmuir, C., Klein, E., Plank, T., 1992. Petrological systematics of mid-ocean ridge basalts: constraints on melt generation beneath ocean ridges. Mantle Flow and Melt Generation at Mid-ocean Ridges. American Geophysical Union, Geophysical Monograph, 71, pp. 183–280.

Le Bas, M.J., Le Maitre, R.W., Streckeisen, A., Zanettin, B., 1986. A chemical classification of volcanic rocks based on the total alkali-silica diagram. Journal of Petrology 27, 745–750.

Le Fevre, B., 2002. Développements chimiques et instrumentaux en géochimie, en vue des analyses isotopiques Lu–Hf et Sm–Nd(Ph.D.) Applications à la géochronologie des roches métamorphiques de haut degréUniversity of Clermont-Ferrand (253 pp.).

Lenoir, X., Garrido, C.J., Bodinier, J.-L., Dautria, J.-M., Gervilla, F., 2001. The recrystallization front of the Ronda peridotite: evidence for melting and thermal erosion of lithospheric mantle beneath the Alboran Basin. Journal of Petrology 42, 141–158.

Liégeois, J.-P., Benhallou, A., Azzouni-Sekkal, A., Yahaoui, R., Bonin, B., 2005. The Hoggar swell and volcanism: reactivation of the Precambrian Tuareg shield during Alpine convergence and West African Cenozoic volcanism. In: Foulger, G.R., Natland, J.H., Presnall, D.C., Anderson, D.L. (Eds.), Plates, Plumes and Paradigms. Geological Society of America Special Paper, 388, pp. 379–400.

Lucassen, F.,Franz, G., Romer, R.L.,Pudlo, D., Dulski, P., 2008. Nd, Pb and Sr isotope composition of Late Mesozoic to Quaternary intra-plate magmatism in NE-Africa (Sudan, Egypt); high-μ signatures from the mantle lithosphere. Contributions to Mineralogy and Petrology 156, 765–784.

Luhr, J.F., Aranda-Gomez, J.J., Housh, T.B., 1995. San Quintin Volcanic Field, Baja Califonia norte, Mexico: geology, petrology and geochemistry. Journal of Geophysical Research 100, 10353–10380.

Lustrino, M., Wilson, M., 2007. The Circum-Mediterranean anorogenic Cenozoic igneous province. Earth Science Reviews 81, 1–65.

Lustrino, M., Duggen, S., Rosenberg, C.L., 2011. The central-western Mediterranean: anomalous igneous activity in an anomalous collisional tectonic setting. Earth Science Reviews 104, 1–40.

Malarkey, J., Wittig, N., Pearson, D.J., Davidson, J., 2011. Characterising modal metasomatic processes in young continental lithospheric mantle: a microsampling isotopic and trace element study on xenoliths from the Middle Atlas Mountains, Morocco. Contributions to Mineralogy and Petrology 162, 289–302.

Maury, R.C., Fourcade, S., Coulon, C., El Azzouzi, M., Bellon, H., Coutelle, A., Ouabadi, A., Semroud, B., Megartsi, M., Cotten, J., Belanteur, O., Louni-Hacini, A., Piqué, A., Capdevila, R., Hernandez, J., Rehault, J.P., 2000. Post-collisional Neogene magmatism of the Mediterranean Maghreb margin: a consequence of slab breakoff. Comptes Rendus de l'Académie des Sciences, Paris, série II 331, 159–173.

Merle, O., Michon, L., 2001. The formation of the West European Rift: a new model as exemplified by the Massif Central area. Bulletin de la Société Géologique de France 172, 213–221.

Middlemost, E.A.K., 1975. The basalt clan. Earth Science Reviews 11, 337–364.

Miller, M.S., Becker, T.W., 2014. Reactivated lithospheric-scale discontinuities localize dynamic uplift of the Moroccan Atlas Mountains. Geology 42, 35–38.

Missenard, Y., Cadoux, A., 2012. Can Moroccan Atlas lithospheric thinning and volcanism be induced by edge-driven convection? Terra Nova 24, 27–33.

Missenard, Y.,Zeyen, H.,Frizon de Lamotte, D., Leturmy, P.,Petit, C., Sébrie, r M., Saddiqi, O., 2006. Crustal versus asthenospheric origin of relief of the Atlas Mountains of Morocco. Journal of Geophysical Research 111, B03401. http://dx.doi.org/10.129/2005JB003708.

Moukadiri, A., Bouloton, J., 1998. Pétrologie des granulites exhumées par le volcanisme récent du Moyen Atlas: aperçu sur la croûte inférieure néogène du Maroc central. Comptes Rendus de l'Académie des Sciences, Paris, série II 327, 731–734.

Moukadiri, A., Pin, C., 1998. Géochimie (éléments majeurs et terres rares) des granulites métasédimentaires en xénolithes dans les basaltes alcalins quaternaires du Moyen Atlas (Maroc): arguments en faveur de la nature pour partie restitique de la croûte inférieure. Comptes Rendus de l'Académie des Sciences, Paris, série II 327, 589–595.

Munker, C.,Pfander, J.A.,Weyer, S.,Büchl, A.,Kleine, T.,Mezger, K., 2003. Evolution of planetary cores and the earth–moon system from Nb/Ta systematics. Science 301, 84–87.

Natali, C.,Beccaluva, L.,Bianchini, R.M.,Siena, F.,Stuart, F.M., 2013. Carbonated alkali–silicate metasomatism in the North Africa lithosphere: evidence from Middle Atlas spinel–lherzolites, Morocco. Journal of South American Earth Sciences 41, 113–121.

Niida, K., Green, D.H., 1999. Stability and chemical composition of pargasitic amphibole in MORB pyrolite under upper mantle conditions. Contributions to Mineralogy and Petrology 135, 18–40.

Oyarzun, R.,Doblas, M.,Lopez-Ruiz, J.,Cebria, J.M., 1997. Opening of the central Atlantic and asymmetric mantle upwelling phenomena: implications for long-lived magmatism in western North Africa and Europe. Geology 25, 727–730.

Panter, K.S., Blusztajn, J., Hart, S.R., Kyle, P.R., Esser, R., McIntosh, W.C., 2006. The origin of HIMU in the SW Pacific: evidence from intraplate volcanism in Southern New Zealand and subantarctic islands. Journal of Petrology 47, 1673–1704.

Pfänder, J.A., Münker, C., Stracke, A., Mezger, K., 2007. Nb/Ta and Zr/Hf in ocean island basalts — implications for crust–mantle differentiation and the fate of niobium. Earth and Planetary Science Letters 254, 158–172.

Pfänder, J.A., Jung, S., Münker, C., Stracke, A., Mezger, K., 2012. A possible high Nb/Ta reservoir in the continental lithospheric mantle and consequences on the global Nb budget — evidence from continental basalts from Central Germany. Geochimica et Cosmochimica Acta 77, 232–251.

Pik, R.,Marty, B.,Hilton, D.R., 2006. How many plumes in Africa? The geochemical point of view. Chemical Geology 226, 100–114.

Pilet, S., Hernandez, J., Bussy, F., Sylvester, P.J., 2004. Short-term metasomatic control of Nb/Th ratios in the mantle sources of alkali basalts. Geology 32, 113–116.

Pilet, S., Baker, M.B., Stolper, E.M., 2008. Metasomatized lithosphere and the origin of alkaline lavas. Science 320, 916–919.

Pilet, S., Ulmer, P., Villiger, S., 2010. Liquid line of descent of a basanitic liquid at 1.5 GPa: constraints on the formation of metasomatic veins. Contributions to Mineralogy and Petrology 159, 621–643.

Pin, C., Briot, D., Bassin, C., Poitrasson, F., 1994. Concomitant separation of strontium and samarium–neodymium for isotopic analysis in silicate samples, based on specific extraction chromatography. Analytica Chimica Acta 298, 209–217.

Piromallo, C., Gasperini, D., Macera, P., Facenna, C., 2008. A late Cretaceous contamination episode of the European–Mediterranean mantle. Earth and Planetary Science Letters 268, 15–27.

Rachdi, H.N., Velde, D., Hernandez, J., 1985. L'association volcanique plio-quaternaire basanite-néphélinite-phonolite du Maroc central. Comptes Rendus de l'Académie des Sciences, Paris, série II 301, 1293–1298.

Raffone, N., Chazot, G., Pin, C., Vanucci, R., Zanetti, A., 2009. Metasomatism in the lithospheric mantle beneath Middle Atlas (Morocco) and the origin of Fe- and Mg-rich wehrlites. Journal of Petrology 50, 197–249.

Rimi, A., 2001. Carte du gradient géothermique au Maroc. Bulletin de l'Institut Scientifique de Rabat 23, 1–6.

Rooney, T.O., Nelson, W.R., Dosso, L., Furman, T., Hanan, B., 2014. The role of continental lithosphere metasomes in the production of HIMU-like magmatism on the northeast African and Arabian plates. Geology 42 (5), 419–422.

Rudnick, R.L., Fountain, M., 1995. Nature and composition of the continental crust — a lower crustal perspective. Reviews in Geophysics 33, 267–309.

Sakuyama, T., Tian, W., Kimura, J., Fukao, Y., Hirahara, Y., Takahashi, T., Senda, R., Chang, Q., Miyazaki, T., Obayashi, M., Kawabata, H., Tatsumi, Y., 2013. Melting of dehydrated oceanic crust from the stagnant slab and of the hydrated mantle transition zone:

constraints from Cenozoic alkaline basalts in eastern China. Chemical Geology 359, 32–48.

Salters, V.J.M., White, W.M., 1998. Hf isotope constraints on mantle evolution. Chemical Geology 145, 447–460.

Sen, G., Keshav, S., Bizimis, M., 2005. Hawaiian mantle xenoliths and magmas: composition and thermal character of the lithosphere. American Mineralogist 90, 871–887.

Sobolev, S.V., Zeyen, H., Granet, M., Achauer, U., Bauer, C., Werling, F., Altherr, R., Fuchs, K., 1997. Upper mantle temperatures and lithosphere–asthenosphere system beneath the French Massif Central constrained by seismic, gravity, petrologic and thermal observations. Tectonophysics 275, 143–164.

Spath, A.,Le Roex, A.,Opiyo-Akech, N., 2001. Plume–lithosphere interaction and the origin of continental rift-related alkali volcanism — the Chyulu Hills volcanic province, southern Kenya. Journal of Petrology 42, 765–787.

Sun, S.S., McDonough, W.F., 1989. Chemical and isotopic systematics of oceanic basalts: implications for mantle composition and processes. In: Saunders, A.D., Norry, M.J. (Eds.), Magmatism in the Ocean Basins. Geological Society of London Special Publication, 42, pp. 313–345.

Teixell, A., Ayarza, P., Zeyen, H., Fernandez, M., Arboleya, M.-L., 2005. Effects of mantle upwelling in a compressional setting: the Atlas Mountains of Morocco. Terra Nova 17, 456–461.

Wagner, C., Mokhtari, A., Deloule, E., Chabaux, F., 2003. Carbonatite and alkaline magmatism in Taourirt (Morocco): petrological, geochemical and Sr–Nd isotope characteristics. Journal of Petrology 44, 937–965.

Walter, M.J.,Katsura, T.,Kubo, A.,Shinmei, T.,Nishikawa, O.,Ito, E.,Lesher, C.,Kunakoshi, K., 2002. Spinel–garnet lherzolite transition on the system $CaO–MgO–Al_2O_3–SiO_2$ revisited: an in-situ X-ray study. Geochimica et Cosmochimica Acta 66, 2109–2122.

Weaver, B.L., 1991. The origin of ocean island end-member compositions: trace element and isotopic constraints. Earth and Planetary Science Letters 104, 381–397.

Weinstein, Y.,Navon, O.,Altherr, R.,Stein, M., 2006. The role of lithospheric mantle heterogeneity in the generation of Plio-Pleistocene alkali basaltic suites from NW Harrat Ash Shaam, Israel. Journal of Petrology 47, 1017–1050.

Wilson, M., Bianchini, G., 1999. Tertiary–Quaternary magmatism within the Mediterranean and surrounding regions. Geological Society of London, Special Publication 156, 141–168.

Wilson, M., Downes, H., 1992. Mafic alkali magmatism associated with the European Cenozoic rift system. Tectonophysics 208, 173–182.

Wilson, M., Downes, H., 2006. Tertiary–Quaternary intra-plate magmatism in Europe and its relationship to mantle dynamics. In: Stephenson, R., Gee, D. (Eds.), European Lithosphere Dynamics. Geological Society of London Memoir, 32, pp. 137–146.

Wittig, N.,Pearson, D.G.,Baker, J.A.,Duggen, S.,Hoernle, K., 2010a. A major element, PGE and Re–Os isotope study of Middle Atlas (Morocco) peridotite xenoliths: evidence for coupled introduction of metasomatic sulphides and clinopyroxene. Lithos 115, 15–26.

Wittig, N.,Pearson, D.G.,Duggen, S.,Baker, J.A.,Hoernle, K., 2010b. Tracing the metasomatic and magmatic evolution of continental mantle roots with Sr, Nd, Hf and Pb isotopes: a case study of Middle Atlas (Morocco) peridotite xenoliths. Geochimica et Cosmochimica Acta 74, 1417–1435.

Xie, S., Tackley, P., 2004. Evolution of U–Pb and Sm–Nd systems in numerical models of mantle convection and plate tectonics. Journal of Geophysical Research 109. http://dx.doi.org/10.1029/2004JB003176.

Zindler, A., Hart, S.R., 1986. Chemical geodynamics. Annual Review of Earth and Planetary Sciences 14, 493–571.